ACS APPLIED MATERIALS & INTERFACES

www.acsami.org

Research Article

Membrane–Electrolyte System Approach to Understanding Ionic Conductivity and Crossover in Alkaline Flow Cells

Thomas Y. George, Isabelle C. Thomas, Naphtal O. Haya, John P. Deneen, Cliffton Wang, and Michael J. Aziz*

Cite This: https://doi.org/10.1021/acsami.3c14173

Read Online

ACCESS | Metrics & More | Article Recommendations | Supporting Information

ABSTRACT: Membrane transport properties are crucial for electrochemical devices, and these properties are influenced by the composition and concentration of the electrolyte in contact with the membrane. We apply this general membrane–electrolyte system approach to alkaline flow batteries, studying the conductivity and ferricyanide crossover of Nafion and E-620. We report undetectable crossover for as-received Nafion and E-620 after both sodium and potassium exchange but high ferricyanide permeability of 10^{-7} to 10^{-8} cm^2 s^{-1} for Nafion subjected to pretreatment prevalent in the flow battery literature. We show how the electrolyte mass fraction in hydrated membranes regulates the influence of ion concentration on membrane conductivity, identifying that increasing electrolyte concentration may not increase membrane conductivity even when it increases electrolyte conductivity. To illustrate this behavior, we introduce a new metric, the membrane penalty, as the ratio of the conductivity of the electrolyte to that of the membrane equilibrated with the electrolyte. We discuss the trade-off between flow battery volumetric capacity and areal power density that arises from these findings. Finally, we apply insights from this approach to provide recommendations for use of membranes in alkaline flow cells and electrochemical reactors in general.

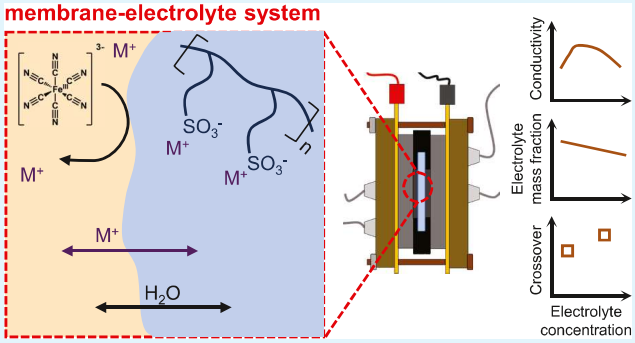

KEYWORDS: *ion-exchange membrane, Nafion, crossover, conductivity, equilibrium, redox flow battery, electrolyte, solubility*

INTRODUCTION

Electrochemical flow cells are poised to play a crucial role in a variety of important electrification and decarbonization efforts from electrolyzers for green chemical synthesis to fuel cells for energy conversion and flow batteries for long-duration energy storage.[1] Membranes, particularly ion-exchange membranes, are at the center of these devices, where they serve to separate the two electrodes where redox reactions occur while enabling conductivity of charge-carrying ions to complete the electrochemical circuit. Research intensified on the transport properties of these membranes along with the development of hydrogen/oxygen fuel cells; consequently, perfluorinated sulfonic acid ionomers, such as Nafion, which are extremely chemically stable and excellent proton conductors in acidic conditions, have become the most widely known and deeply studied cation-exchange membranes.[2]

The broadening applications of electrochemical cells call for a thorough understanding of ion-exchange membrane properties in diverse chemical environments in order to synchronize the development of next-generation materials with the design of new technology. Redox flow batteries (RFBs) constitute a case in which this approach could be particularly significant. The all-vanadium redox flow battery, with the V^{4+}/V^{5+} redox couple in the posolyte and V^{3+}/V^{2+} in the negolyte, aqueous acidic supporting electrolyte, and typically a proton-conducting cation-exchange membrane, is presently the most developed RFB technology.[3,4] Water-soluble synthetic redox reactants, including organic molecules,[5−7] oligomers,[8,9] and polymers,[10] as well as metalorganic[11−14] and inorganic complexes,[15−17] attract research and commercial attention to replace or supplement incumbent vanadium technology. The synthetic redox reactants offer tunable properties, potentially sustainable synthesis[18] and feedstocks,[19] and recently, extremely low capacity fade rates.[20] The most stable synthetic redox reactants, however, are both stable and soluble only in neutral or alkaline conditions, where typically alkali metal cations carry charge through a cation-exchange membrane.[21−26] Here, we adopt a membrane–electrolyte system approach to understanding membrane properties in flow cells, with the

Received: September 21, 2023
Revised: November 21, 2023
Accepted: November 25, 2023

recognition that a system including an electrolyte contacting a membrane will tend toward a two-phase equilibrium that governs the uptake of solvent into the membrane pores, the partitioning and exchange of ions,[27] and hence the morphology and transport properties of the membrane phase.[2,28,29] Properties of an electrolyte, e.g., redox reactant concentration, pH, supporting electrolyte concentration, and the charge-carrying ion, affect the intricate energy balance determining the system equilibrium, and we propose that this introduces trade-offs in electrochemical reactor design and opportunities for improvement.

The role of an RFB membrane is to suppress the crossover of redox reactants to the wrong side of the battery, which results in capacity and Coulombic efficiency loss while providing high conductivity of charge-carrying ions to minimize the cell resistance and provide high voltage efficiency and areal power density.[30,31] Because crossover species and charge-carrying ions must each take transport paths through the hydrated membrane pores, efforts toward decreasing membrane resistance tend to concomitantly increase crossover. For most flow batteries that comprise negolytes and posolytes with different chemicals (vanadium RFBs being a notable exception because they comprise vanadium in four different oxidation states), crossover leads to capacity loss that cannot be recovered without a burdensome chemical purification process, and it is particularly important for crossover to be reduced to nearly negligible rates.

Despite being developed for acidic conditions, Nafion remains the most commonly reported cation-exchange membrane in the flow battery literature, including in neutral and alkaline flow cells. For a given water content, the proton conductivity of Nafion is a factor of ten higher than that of any alkali metal cation[2] and, as a result, low area-specific resistance and high power density have been difficult to realize with emerging synthetic flow battery chemistries utilizing alkali metal charge carriers.[32−34] Besides Nafion, Fumasep E-620 (and other E-600 series membranes of different thicknesses) is an increasingly popular commercial cation-exchange membrane used in lab-scale flow batteries. E-620 is reported to be a sulfonated poly(aryl ether ketone) membrane, and it has attracted attention because its nonfluorinated polymer chemistry is potentially low cost,[21] and it is readily available as films that are relatively thin (E-620 and E-610 are 20 and 10 μm thick, respectively) that can provide low resistance in a battery.[35] Nonetheless, the transport properties of the E-600 series membranes have yet to be systematically characterized.

In the present work, we showcase a set of membrane characterization methods that are widely accessible and reproducible and enable rapid iteration while still providing some fundamental insight into how electrolyte properties affect the membrane structure and function. As the main measurable quantities to describe the membrane−electrolyte system, we select conductivity (mS cm^{-1}) and permeability to crossover of a redox-active species (cm^2 s^{-1}), as the key transport properties of ions in the membrane, and electrolyte mass fraction (%), the mass fraction of imbibed electrolyte in a hydrated membrane, as a descriptor of relatively how much of the hydrated membrane structure is available as a transport medium. Electrolyte mass fraction is reckoned as $(m_{wet} - m_{dry})/m_{wet} \times 100\%$, where m is the mass. We select Nafion N117 and NR212 and Fumasep E-620 as materials to study because they are the most widely used commercially available membranes for alkaline RFBs. For the electrolytes in our membrane−electrolyte system, here, we explore conditions relevant to alkaline flow batteries, a system for which membrane properties are least investigated. We use sodium and potassium hydroxide, or their mixture, as supporting (not redox active in a battery) electrolytes. We study iron (II/III) hexacyanide (ferrocyanide/ferricyanide, respectively) as representative redox reactants; ferricyanide is typically the fastest-crossing species when paired against an organic redox couple. For the set of cation-exchange membranes and electrolyte species considered in this work, sodium and potassium are counterions with respect to the membrane phase (oppositely charged to the negatively charged sulfonate moieties in the membrane), whereas the iron hexacyanide anions are co-ions. We also investigate the effect of pretreatment on Nafion, comparing a treatment of hot water followed by dilute hydrogen peroxide at room temperature, as described in the literature,[36−48] to using membranes as-received.

We evaluate the effects of supporting salt concentration (i.e., pH), cations (Na^+, K^+, and mixtures of both), and iron hexacyanide concentration on conductivity and on ferricyanide permeability through E-620 (as-received) and through Nafion (pretreated and as-received). Taken together, the results underscore the benefits of the membrane−electrolyte system approach as a way to connect membrane transport phenomena with electrolyte composition, evaluate trade-offs, and guide future research. While the results are specific to the system selected, we maintain that the methods and theoretical framework are general and transferable to all flow reactors with perm-selective membranes.

MATERIALS AND METHODS

Chemicals and Materials. Potassium ferrocyanide trihydrate, sodium ferrocyanide decahydrate, and potassium ferricyanide were purchased from Sigma-Aldrich. 2,5-Dihydroxy-1,4-benzoquinone was purchased from Sigma-Aldrich. Nafion membranes were purchased from Ion Power. Fumasep E-620 membranes were graciously provided by Dr. Bernd Bauer of Fumatech free of charge. Sigracet GDL 39AA electrodes were purchased from the Fuel Cell Store.

Membrane Pretreatment. All membranes referred to as "pretreated" in this work were soaked for 20 min in deionized water at 80 °C, followed by 35 min soaked in 5% hydrogen peroxide in water at room temperature.[38] Otherwise, membranes were used as-received.

Membrane Conductivity and Electrolyte Mass Fraction. Following pretreatment (if applicable), each membrane piece was transferred to soak in the electrolyte for study overnight. Three pieces of the same type of membrane per distinct experimental condition were prepared in the same solution for triplicate measurements.

After soaking in the electrolyte, each membrane piece was assembled into flow cell hardware (Figure S1). Flow cell hardware was graciously provided by Prof. Fikile Brushett (JCESR Gen. 2 flow cell, active area of 2.55 cm^2). Sigracet GDL 39AA electrodes were manually cut to size and otherwise used as-received. Bolts to compress the cell were tightened with 10−12 in-lb. torque using a torque wrench. The same electrolyte in which membranes were soaked was then circulated through both sides of the cell at 50−60 mL min^{-1} using a Masterflex variable speed peristaltic pump (Figure S2).

The resistance of the cell was measured with potentiostatic electrochemical impedance spectroscopy at an open circuit, with a 10 mV rms AC perturbation in the frequency range of 100 Hz to at least 200 kHz using a Gamry Reference 3000 potentiostat. In some cases, the high-frequency limit was increased up to 1 MHz to clarify the high-frequency resistance. The resistance of the cell assembled in the same way but without the membrane was also measured with the same technique and was found to be 0.05−0.13 Ω. The average shorted cell resistance (0.09 Ω) was subtracted from each

https://doi.org/10.1021/acsami.3c14173
ACS Appl. Mater. Interfaces XXXX, XXX, XXX−XXX

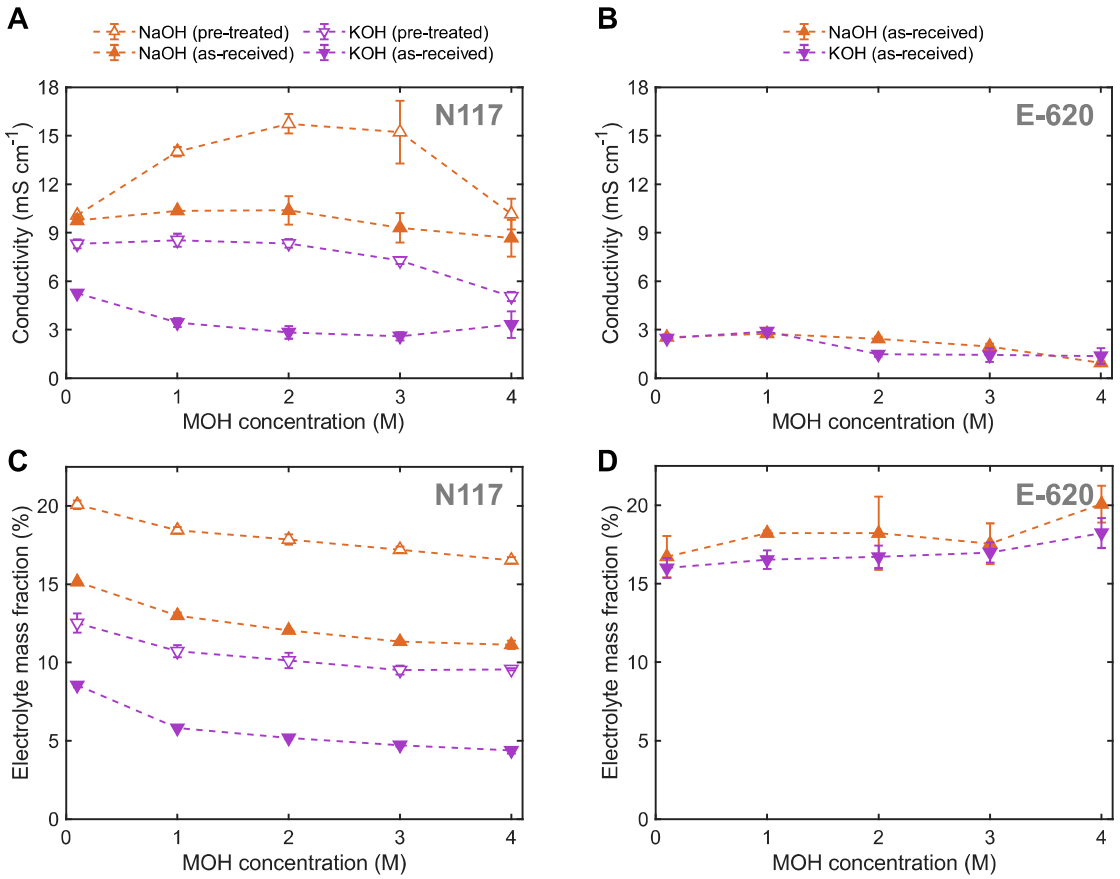

Figure 1. Conductivity (A, B) and electrolyte mass fraction (C, D) of Nafion N117 (A, C) and Fumasep E-620 (B, D) membranes soaked in NaOH or KOH electrolytes at select concentrations (M in MOH represents Na or K). Corresponding data are listed in Tables S2 and S3.

measurement of cell resistance with a membrane to approximate the resistance contribution from the membrane. This value was converted to conductivity by using the nominal membrane thickness (183 μm for Nafion N117 or 20 μm for E-620) and the active area of the cell. Vertical error bars for conductivity are standard deviations from the average of the three conductivity values per experimental condition.

Following the measurement of resistance, membranes were transferred back to their respective electrolytes to soak again for at least 5 h. Then, m_{wet} was measured by first gently drying the surface of the piece of membrane by dragging it across the surface of a stack of lint-free lab wipes (taking care to neither squeeze out water within the membrane by blotting it nor leave behind surface water droplets) and next measuring the mass with an analytical balance (METTLER TOLEDO). Finally, each membrane was dried at least overnight in an oven at 100 °C and then quickly weighed on an analytical balance to obtain m_{dry}. Electrolyte mass fraction was determined as $(m_{wet} - m_{dry})/m_{wet} \times 100\%$, which was determined for each unique sample and then reported as the average of the three samples per distinct experimental condition. Vertical error bars for the electrolyte mass fraction are standard deviations of the average.

Permeability. Permeability was evaluated by using custom glass H-cells from Adams and Chittenden. In this setup, membranes were clamped between a donor and a receiving electrolyte, each 10 mL in volume. Nafion NR212 was pretreated as specified and then soaked at least overnight in 1 M MCl at pH 12 for ion exchange, whereas E-620 was loaded dry as customary for use in flow batteries. Electrolyte compositions are specified in Results and Discussion section: Crossover Depends on Pretreatment. Sodium ferricyanide electrolytes were prepared as specified in Materials and Methods section: Preparation of Sodium Ferricyanide Electrolytes. Three H-cells were assembled per unique experimental condition for triplicate measurements (Table S1).

During a given experiment, H-cells were housed under a tent of tinfoil or a cardboard box to avoid the known dissociation of iron cyanide complexes in sunlight.[49] Electrolytes in the H-cells were continuously stirred on a multichannel magnetic stir plate (Scilogex). Aliquots were periodically taken from the H-cell receiving electrolytes, diluted in a cuvette as needed, and the concentration of ferricyanide was measured using UV–vis spectrophotometry (Agilent) and a previously established calibration curve.[50] Volume removed by the aliquot was replaced with pristine receiving solution, and the resulting dilution of the receiving side was accounted for in the determination of permeability from concentration measurements by the procedure established in our group.[51]

Electrolyte Conductivity. Conductivity of electrolytes was measured using an Orion two-electrode probe (018020MD) connected to an Orion Star A215 pH/conductivity benchtop multiparameter meter (both purchased from ThermoFisher). The cell constant of the conductivity probe was calibrated using an Orion 111.9 mS cm^{-1} conductivity standard. Electrolyte conductivity measurements were done at room temperature; the temperature of the electrolytes ranged from 23 to 24 °C.

Ferrocyanide Solubility with Mixed Counterions. Saturated ferrocyanide solutions with a defined Na^+/K^+ ratio were prepared by mixing $K_4Fe(CN)_6$ and $Na_4Fe(CN)_6$ salts and adding an aqueous solution of NaOH and KOH with the target ratio until most ferrocyanide salts dissolved but a small precipitate persisted. Then, the precipitate was suspended in the solution and filtered with Whatman paper. The ferrocyanide concentration of the filtrate was determined by UV–vis spectrophotometry and a previously established calibration curve.[50] The filter paper was dried in air, and the mass of the filter paper with filtered precipitates was measured with an analytical balance (METTLER TOLEDO). Figure S3 shows a photograph of an example filter paper from this process. Subtracting

https://doi.org/10.1021/acsami.3c14173
ACS Appl. Mater. Interfaces XXXX, XXX, XXX−XXX

the previously measured mass of the pristine filter paper gave the mass of precipitates. Using the mass of precipitates, horizontal error bars on the Na^+/K^+ ratio were determined, assuming the precipitate was either entirely $Na_4Fe(CN)_6$ or entirely $K_4Fe(CN)_6$ (this error is zero for Na^+/K^+ ratio of zero or unity). Solubility experiments were done at room temperature, which at the time ranged from 18 to 22 °C.

Preparation of Sodium Ferricyanide Electrolytes. Sodium ferricyanide was prepared by bulk electrolysis of sodium ferrocyanide, using redox flow battery hardware (Fuel Cell Technologies Inc.) and cell compression conditions typical to our group.[16] Nafion N117, soaked overnight in 1 M NaOH and then rinsed and stored in deionized water, was used as the membrane. Sodium ferrocyanide at an approximately 0.53 M concentration in water was prepared as the capacity-limiting positive electrolyte. The negolyte redox reactant was 2,5-dihydroxy-1,4-benzoquinone,[52] provided in excess for approximately twice the capacity (coulombs) as the posolyte. The composition of the negolyte was approximately 0.05 M 2,5-dihydroxy-1,4-benzoquinone at pH 13 (pH adjusted with NaOH), with the concentration of benzoquinone limited by its solubility in the sodium electrolyte. The cell was charged by applying 1.6 V until the current dropped to 10 mA (2 mA cm^{-2}) to allow for a nearly complete conversion of ferrocyanide to ferricyanide in the posolyte. The concentration of sodium ferricyanide following bulk electrolysis was confirmed to be 0.6 M by UV–vis spectrophotometry, and then, the pH was adjusted to 12 with NaOH for use in crossover experiments. For crossover experiments with a 0.2 M donor electrolyte, this sample was diluted as needed.

RESULTS AND DISCUSSION

Supporting Electrolyte Affects Membrane Conductivity. We first consider Nafion (as-received and pretreated) and E-620 (as-received) that have been soaked in the supporting electrolyte (sodium hydroxide or potassium hydroxide) at different concentrations in the absence of redox reactants that would be present in a battery electrolyte. All membranes referred to as "pretreated" in this work were subjected to the same treatment: 20 min soaked in deionized water at 80 °C followed by 35 min soaked in 5% hydrogen peroxide in water at room temperature.[38] As-received and pretreated membranes alike were then transferred to soak in selected electrolytes at least overnight before measuring conductivity and electrolyte mass fraction (see Materials and Methods section). Over the course of the soaking time, ions were exchanged between the membrane and contacting electrolyte, electrolyte liquid was absorbed by the membrane to form hydrated pores, and the physical structure of the polymer was adjusted to accommodate the imbibed solute and solvent species, as the membrane–electrolyte system approached two-phase equilibrium. In the case of Nafion, the sulfonic acid groups initially present were neutralized by hydroxide and exchanged with sodium or potassium. E-620 was initially received with potassium counterions, also known as E-620(K). To improve the precision of electrolyte mass fraction measurements, Nafion N117 (nominally 183 μm thick), one of the thickest available membranes of the Nafion polymer, was studied, but the properties we report in this work are all thickness-independent (other than due to any microstructural changes from differences in manufacturing).[53,54]

Figure 1A shows the dependence of Nafion N117 conductivity on cation species (Na^+ or K^+), concentration, and pretreatment. As the concentration of the alkali metal hydroxide (MOH) in the contacting electrolyte increases, starting from 0.1 M, the conductivity of both pretreated and as-received Nafion N117 in NaOH initially increases. Then, with further increasing concentration of NaOH, conductivity begins to decrease from a maximum conductivity at 2–3 M for pretreated Nafion N117 and 1–2 M for as-received Nafion N117. Meanwhile, electrolyte mass fraction decreases monotonically with the concentration for both pretreated and as-received Nafion N117 in NaOH (Figure 1C). We interpret the results in Figure 1 with these concepts: increasing the concentration of mobile ions tends to increase conductivity through any available pathway, while simultaneously decreasing the electrolyte mass fraction reduces the number of available transport pathways. These factors compete, leading to a NaOH concentration at which conductivity is maximized. A similar phenomenon was reported for Nafion N117 (with a pretreatment similar to that of the pretreated membranes reported here) soaked in sulfuric acid, in which the water content of the membrane decreased with increasing sulfuric acid concentration and the membrane conductivity was maximized around 3 M sulfuric acid and decreased with concentrations greater than that.[55] Also, an early study on Nafion 110 that was pretreated in boiling water for 30 min found that the membrane water content decreased linearly between 1 and 5 M sodium chloride in the contacting electrolyte and the conductivity was maximized at 3 M sodium chloride.[56]

Figure 1 also shows that Nafion N117 conductivity only decreases, or is approximately constant within error, with increasing KOH concentration from 0.1 to 4 M in the contacting electrolyte, regardless of pretreatment, and that electrolyte mass fraction also decreases with concentration. This is unlike the trend for Nafion that was sodium-exchanged but is consistent with a previous report comparing conductivity and water content of Nafion N117 in NaCl and KCl electrolytes.[57] Electrolyte mass fraction for potassium-exchanged Nafion is lower than that for sodium-exchanged Nafion. Sodium is a smaller ion than potassium, but both have +1 charge, so sodium has a higher surface charge density and more strongly coordinates water compared to potassium. Therefore, sodium ions bring more water to form the pores of the hydrated membrane.

The results reported here suggest how the electrolyte mass fraction of the membrane influences the trend of conductivity with the concentration of the contacting electrolyte. Pretreated sodium-exchanged Nafion N117 exhibits the highest electrolyte mass fractions and the highest conductivity across the range of concentrations studied and also exhibits the highest concentration of MOH in the contacting electrolyte beyond which conductivity no longer increases. As-received potassium-exchanged Nafion N117 has the lowest electrolyte mass fractions and lowest conductivity across the range of concentrations, and conductivity decreases only with increasing concentration in the contacting electrolyte. For a given counterion (here meaning Na^+ or K^+), pretreatment increases electrolyte mass fraction and conductivity of Nafion; although there is no clear increase in conductivity with KOH concentration for pretreated Nafion, there is a much sharper decrease in conductivity between 0.1 and 1 M KOH for as-received potassium-exchanged Nafion. The hydrogen peroxide in the pretreatment is intended to clean impurities from manufacture and transport from the membrane. Heating Nafion in water has been shown to establish a thermal history that determines the morphology of the hydrated polymer, because of which, higher pretreatment temperatures cause subsequently higher water content.[2]

https://doi.org/10.1021/acsami.3c14173
ACS Appl. Mater. Interfaces XXXX, XXX, XXX–XXX

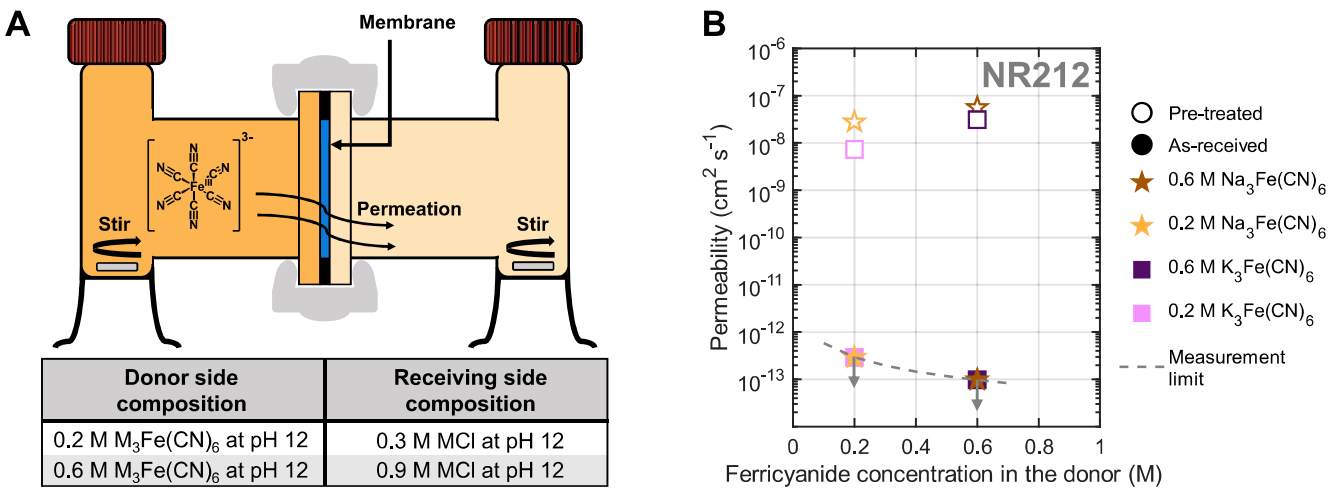

Donor side composition	Receiving side composition
0.2 M $M_3Fe(CN)_6$ at pH 12	0.3 M MCl at pH 12
0.6 M $M_3Fe(CN)_6$ at pH 12	0.9 M MCl at pH 12

Figure 2. (A) Schematic H-cell setup for measuring ferricyanide permeability with a table below specifying the electrolyte composition on the receiving side for a given ferricyanide concentration in the donor. M represents Na or K. (B) Permeability of ferricyanide through pretreated and as-received Nafion NR212.

E-620 shows a lower conductivity and higher electrolyte mass fraction than Nafion N117 for most of the conditions studied. The conductivity results emphasize that the relatively low resistance reported for flow batteries using E-600 series membranes[21−23,26,58,59] is mainly due to the membrane thickness. Because Nafion and E-620 are different polymers with different densities, it is less useful to compare the electrolyte mass fraction between the two polymers than it is to compare between different electrolyte conditions and the same polymer. The most notable difference between the Nafion and E-620 results is that the properties of Nafion are strongly influenced by its counterion, but the influence is negligible for E-620. The structure of Nafion includes flexible side chains terminating in ion-exchange sites (hydrophilic sulfonate moieties) tethered to the hydrophobic backbone. These flexible side chains are free to undergo significant rearrangement as a function of cation exchange.[2,50] Complementary small-angle X-ray[60,61] and neutron[62] scattering experiments have characterized the structure of water domains in hydrated Nafion exchanged with various cations and have shown that both the sizes of individual water domains and the structure of the hydrated polymer matrix are influenced by cations.[2] Larger cations favor both smaller and more separated water domains, which supports our observations of lower Nafion conductivity in potassium electrolytes compared to sodium. In contrast to Nafion, our results suggest that the pores that form in hydrated E-620 are relatively rigid, and the polymer does not exhibit significant rearrangement depending on its counterion.

Crossover Depends on Pretreatment. The results in Figure 1 cannot alone determine the ideal membrane/electrolyte/pretreatment combination for use in flow batteries because increasing conductivity may come at the expense of increased crossover. Next, we evaluate the permeability of ferricyanide through pretreated and as-received Nafion NR212 (50 μm thick: a thinner Nafion membrane than N117 was chosen to accelerate crossover measurement), shown in Figure 2, and as-received E-620 (Supplementary Discussion 1). Permeability is an effective diffusion coefficient describing crossover driven by the difference in concentration of the crossing species between a "donor" and "receiving" side of a two-chamber system. Ferricyanide, rather than ferrocyanide, was chosen as the benchmark crossover species because ferricyanide possesses one fewer negative charge per ion, providing weaker charge exclusion from a cation-exchange membrane and hence higher expected permeability.[51] H-cells were assembled with a donating electrolyte containing 0.2 or 0.6 M $M_3Fe(CN)_6$ (where M is either Na or K) at pH 12. The receiving side electrolyte was determined to osmotically balance the two chambers based on freezing-point osmometer measurements on solutions of $K_3Fe(CN)_6$ and KCl.[50] All Nafion regardless of pretreatment was soaked in 1 M MCl at pH 12 at least overnight before the assembly of H-cells. Crossover was measured by periodic UV−vis spectrophotometry of the receiving electrolyte (see Materials and Methods section for details) to determine crossed-over ferricyanide concentrations, which are used in the evaluation of permeability.

The ferricyanide permeability of pretreated Nafion NR212 approximately falls in the range of 10^{-7} to 10^{-8} cm^2 s^{-1}. A permeability of 10^{-7} cm^2 s^{-1} means a lab-scale flow battery with 10 mL ferricyanide electrolyte at 0.2 M concentration and 5 cm^2 membrane area would lose 20% of its capacity from crossover in 6 h. Although the exact impact of crossover on flow battery capacity loss depends on the membrane area relative to the amount of redox-active material, permeability values on this order are clearly too high for battery systems with decadal lifetimes and without crossover recovery methods.

The ferricyanide crossover rate through pretreated Nafion is greater for sodium-exchanged membrane than potassium-exchanged membrane, which can be explained by the relatively higher electrolyte mass fraction of the sodium-exchanged membranes. Additionally, permeability is higher for higher ferricyanide concentrations because higher concentrations of co-ions such as ferricyanide in the contacting electrolyte act to weaken the charge-exclusion effect of the membrane.[51] Data used to calculate permeability of pretreated Nafion are provided in Figure S4 and permeability values are tabulated in Table S1.

In stark contrast to pretreated Nafion, no detectable crossover was observed for as-received Nafion or as-received E-620, regardless of sodium or potassium cations. Figure 2B assigns a measurement limit of 3×10^{-13} cm^2 s^{-1} on permeability through a 50 μm membrane with a donating

https://doi.org/10.1021/acsami.3c14173
ACS Appl. Mater. Interfaces XXXX, XXX, XXX−XXX

species concentration of 0.2 M and 5 days without a UV−vis absorbance measurement above the sensitivity limit for the given crossover species. The equivalent measurement limit for a donor concentration of 0.6 M is 1×10^{-13} cm^2 s^{-1}. For our instrument, a concentration detection limit of 1 μM was previously determined for ferricyanide.[50] Absorbance spectra for triplicate H-cells after 5 days of experiments for the undetectable crossover conditions in Figure 2B are provided in Figure S5. Equivalent data for E-620 are provided in Figure S6; see accompanying Supplementary Discussion 1. Five-day experiments were used as the basis to compare the undetectable crossover conditions presented here, because experiments of this duration for each case could be run without water crossover causing a buildup of pressure to skew the results over time. However, experiments performed with as-received potassium-exchanged Nafion were especially robust against water crossover in the H-cell configuration, and we were able to evaluate these conditions with experiments lasting over 50 days, during which time detectable crossover was *still* not observed (Figure S7). Therefore, the actual permeability of ferricyanide in these cases could be as much as an order of magnitude lower than the limits shown in Figure 2B.

For a lab-scale flow battery with 10 mL, one-electron-transfer-per-molecule (like ferricyanide) electrolyte at 0.2 M concentration and 5 cm^2 membrane area, capacity fade due to crossover through as-received sodium- or potassium-exchanged Nafion would be approximately 1 order of magnitude lower than the 0.02% day^{-1} fade rate target for battery cycling to be considered "extremely stable."[20] In Supplementary Discussion 2, we show a calculation estimating the influence of diffusion-driven crossover permeation on the capacity retention of a flow battery with an 8 h discharge duration and 80% round-trip energy efficiency, which are practical specifications for a system at scale. With permeability of 1×10^{-13} cm^2 s^{-1}, area-specific resistance of 2 Ω cm^2 and membrane thickness of 50 μm (e.g., Nafion NR212), corresponding to 2.5 mS cm^{-1} conductivity, we estimate capacity retention of 85% after 10 years (Figure S8). Although it is important to note that this calculation leaves out realities of charge−discharge cycling such as changes in the state of charge and electric-field-driven crossover mechanisms, the results we report here hold promise for crossover rates low enough to enable practical flow batteries with decadal lifetimes.

Pretreated—not as-received—Nafion has been customarily used as the benchmark to evaluate new membrane candidates for aqueous organic RFBs.[39−48] Many such studies have reported impressive membranes with lower ferricyanide permeability and higher potassium conductivity than pretreated Nafion. But, to the best of our knowledge, only one membrane, a sulfonated poly(phenylene), has matched the undetectable crossover of as-received Nafion NR212 while improving upon its potassium conductivity.[50] We urge that flow battery membrane researchers, especially for aqueous organic RFBs, consider the transport properties of as-received Nafion as more important benchmarks than those of pretreated Nafion. Moreover, we emphasize that the properties of Nafion are extremely pretreatment-dependent, and therefore, all membrane pretreatments should be clearly reported in the main text of manuscripts discussing this material.

Active Species Concentration Affects Membrane Conductivity. Due to the exceptionally low ferricyanide permeability, we select as-received Nafion and E-620 for further evaluation of conductivity and electrolyte mass fraction in representative alkaline RFB electrolytes (Figures 3, S9−S11, and Tables S4−S6). Ferrocyanide, commercially available as sodium and potassium salts, was chosen as the redox reactant present in the electrolyte, and MOH at either 0.01 or 1 M (nominally pH 12 and 14) was used as the supporting electrolyte. Studies with potassium ferricyanide and Nafion N117 were also performed and showed little difference from the ferrocyanide results (Figure S9, Table S5). Ferrocyanide concentrations approaching the solubility limit of each alkali metal salt in the supporting electrolyte were studied.

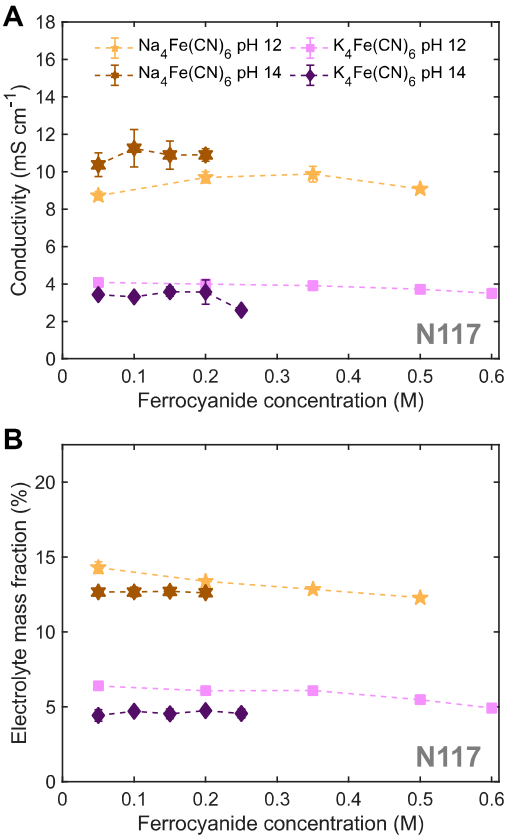

Figure 3. Conductivity (A) and electrolyte mass fraction (B) of Nafion N117 membranes soaked in representative flow battery electrolytes containing ferrocyanide (active species) and either a 0.01 M (pH 12) or 1 M (pH 14) hydroxide supporting electrolyte. Corresponding data are listed in Table S4.

Consistent with the results in just MOH supporting electrolytes, the conductivity and electrolyte mass fraction values of sodium-exchanged Nafion N117 are greater than those for potassium-exchanged Nafion N117 for all cases studied in this section. In all cases, the electrolyte mass fraction is either approximately constant or decreasing with increasing ferrocyanide concentration. Additionally, comparing the pH 12 and 14 conditions for each cation form shows that adding the supporting electrolyte decreases the electrolyte mass fraction in the membrane. The concentration of supporting salt affects the water activity in the electrolyte; adding supporting salt to a concentrated electrolyte lowers the water activity and favors dehydration of the membrane phase, moving water into the contacting electrolyte phase.

The trends of conductivity with supporting electrolyte and ferrocyanide concentration match the electrolyte mass fraction trend for potassium-exchanged Nafion but not for the sodium-

https://doi.org/10.1021/acsami.3c14173
ACS Appl. Mater. Interfaces XXXX, XXX, XXX−XXX

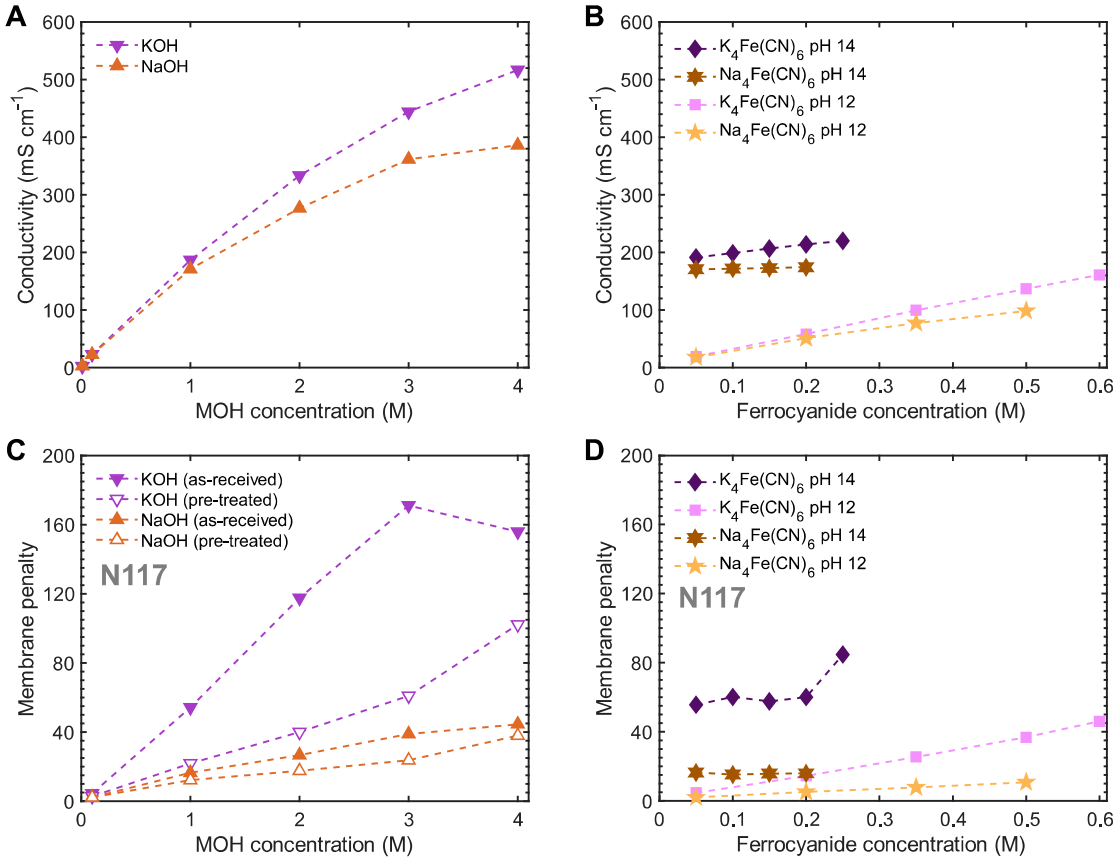

Figure 4. Conductivity of (A) MOH (M represents Na^+ or K^+) and (B) representative flow battery electrolytes containing ferrocyanide. Membrane penalty for (C) MOH electrolytes (pretreated and as-received membranes) and (D) flow battery electrolytes (as-received membranes) with Nafion N117.

exchanged cases. Unlike for potassium-exchanged Nafion, conductivity measurements for sodium-exchanged Nafion at pH 14 show higher sodium conductivity for ferrocyanide-containing electrolytes than at pH 12. Furthermore, the conductivity of sodium-exchanged Nafion increases with ferrocyanide concentration to a point (0.1 M ferrocyanide at pH 14 and 0.35 M ferrocyanide at pH 12) before decreasing at higher concentrations. Nevertheless, the qualitative trends of conductivity with ferrocyanide concentration in Figure 3 match the trends of conductivity with MOH concentration in Figure 1 for both sodium- and potassium-exchanged Nafion. These complementary data sets show that the cationic electrolyte species strongly influences the electrolyte mass fraction of the membrane, which, in turn, regulates the effects of ion concentration on conductivity. Together, these results also complement previous membrane–electrolyte equilibrium studies focused on vanadium RFBs, which show that increased vanadium concentrations in the contacting electrolyte decrease membrane conductivity.[55,63]

Overall, the results indicate that a high concentration of redox reactants, favored for high volumetric capacity batteries, may trade off against membrane conductivity. They also indicate that the supporting salt is not always helpful for increasing membrane conductivity. In fact, conductivity values for Nafion N117 and E-620 in potassium ferrocyanide without any supporting KOH (Figure S11) closely match results from the equivalent experiments at pH 12 (Figures 3 and S7), demonstrating that the supporting salt is not necessary to provide conductivity at ferrocyanide concentrations as low as 50 mM.

Membrane Penalty. The relationship between the ionic conductivity of an electrolyte and of a polymer matrix in equilibrium with that electrolyte (i.e., a polymer electrolyte) is complicated because, for a polymer electrolyte, the concentration and composition of dissolved ions affect the morphology and transport properties of the medium, as we have shown, e.g., in Figures 1–3. Ionic conductivity of an electrolyte is also affected by its concentration and composition, broadly because ion–ion and ion–solvent interactions of nonideal solutions govern the viscosity,[64] which, in turn, has a strong effect on conductivity, which is also further affected by the constraining influences of ion–ion and ion–solvent interactions.[65]

Figure 4A shows that the ionic conductivity of KOH and NaOH electrolytes increases with the concentration up to 4 M, but the increase of conductivity per unit concentration diminishes as the concentration increases, in agreement with the literature.[66,67] Figure 4B shows that the ionic conductivity of representative ferrocyanide-based battery electrolytes with either 0.01 M (pH 12) or 1 M (pH 14) MOH increases linearly with the ferrocyanide concentration approaching the solubility limit in the given supporting electrolyte. Conductivity values of the ferrocyanide-based battery electrolytes at pH 12 approach the conductivity values of pH 14 electrolytes at ferrocyanide concentrations approaching the solubility limits, and the solubility limits for ferrocyanide are maximized here at minimum supporting electrolyte concen-

https://doi.org/10.1021/acsami.3c14173
ACS Appl. Mater. Interfaces XXXX, XXX, XXX–XXX

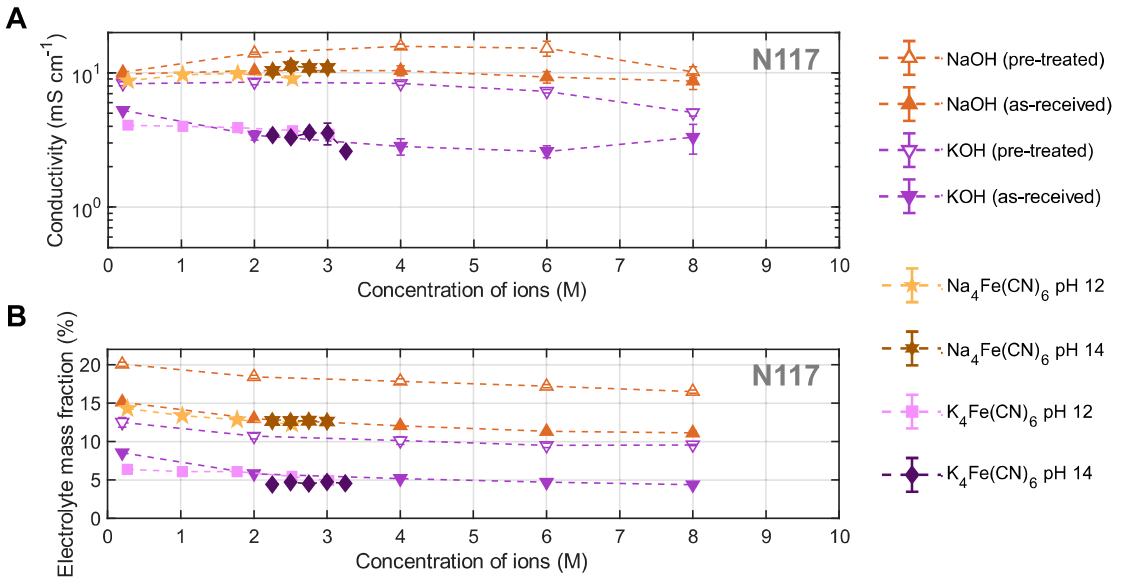

Figure 5. Conductivity (note semilog scale) (A) and electrolyte mass fraction (B) of Nafion N117 soaked in MOH supporting electrolytes (pretreated and as-received membranes) as well as Nafion N117 (as-received) soaked in ferrocyanide flow battery electrolytes, plotted versus total concentration of ions in the contacting electrolyte. Corresponding data are given in Tables S2 and S4.

tration due to the common ion effect. These results underscore that water-soluble ionic synthetic redox reactants for flow batteries can provide good electrolyte conductivity without supporting electrolytes.

We introduce a dimensionless metric, the membrane penalty (eq 1), defined as the conductivity of the electrolyte ($\sigma_{electrolyte}$) divided by the conductivity of the polymer electrolyte or other separator material ($\sigma_{membrane}$) in equilibrium with that electrolyte for a given membrane or separator. The membrane penalty is an analogous metric to the previously proposed dimensionless diffusivity/permeability (D/P or D_{sol}/D_{eff}) ratio that accounts for how the membrane constrains the transport of crossover species compared to the diffusivity of the species in the electrolyte.[40,51,68,69] Indeed, both metrics are inverse examples of MacMullin numbers;[70−73] a MacMullin number is a ratio of the value of a transport parameter (e.g., resistance, conductivity, diffusivity of a species) in a porous medium (e.g., an electrode) to its value in the relevant nonporous medium (e.g., an electrolyte). We hypothesize that the membrane penalty of an uncharged porous separator would be a factor in capturing the porosity and tortuosity of the medium but that the membrane penalty of a polymer electrolyte depends on the intricate membrane−electrolyte equilibrium. While high D/P is desired for low crossover with good mass transport properties of redox reactants, a low membrane penalty is desired for low resistance. We have previously reported how high D/P values may be achieved by leveraging charge exclusion of crossover species,[51] and in this work, we show the dependence of membrane penalty on counterion and concentration. Careful choice of electrolyte composition in conjunction with a crossover-resistant redox reactant and membrane combination may enable both a low membrane penalty and high D/P.

$$\text{membrane penalty} = \frac{\sigma_{electrolyte}}{\sigma_{membrane}} \quad (1)$$

The conductivity of potassium-based electrolytes is higher than that of sodium-based electrolytes with the same MOH and ferrocyanide concentration, whereas Nafion exhibits higher conductivity when sodium-exchanged, implying a greater membrane penalty for potassium than for sodium. The increase of membrane penalty with concentration is steepest when increasing the ion concentration increases electrolyte conductivity but decreases membrane conductivity in contact with that electrolyte. For these reasons, the highest membrane penalties we report are for potassium-exchanged Nafion, and the average slopes of membrane penalty vs concentration (MOH or ferrocyanide) are also highest for potassium-exchanged Nafion (Figure 4C,D). The slope of membrane penalty vs ferrocyanide concentration represents the severity of the trade-off of resistance, which is inversely proportional to a battery's power density, against the battery's volumetric capacity.

Total Ion Concentration Determines Membrane Properties. By examining the dependence of membrane conductivity and electrolyte mass fraction on the total concentration of ions in the contacting electrolyte using the data we have introduced, we are able to draw more general conclusions about this membrane−electrolyte system. We define the concentration of ions as the sum of the concentrations of each ion in the electrolyte assuming complete dissociation of salts, e.g., 0.5 M $K_4Fe(CN)_6$ = 0.5 M × 5 = 2.5 M ions.

In Figure 5, where the conductivity and electrolyte mass fraction of Nafion N117 soaked in MOH or ferrocyanide-based battery electrolytes are plotted against the concentration of ions, the data taken with the same membrane pretreatment and cation exchange are overlapping. Electrolyte mass fraction of these membranes, in general, decreases with the total ion concentration of the contacting electrolyte. Meanwhile, cation exchange and pretreatment are the main determinants of electrolyte mass fraction across the range of ion concentrations studied. Overall, the results show that the effect of ion concentration on conductivity and electrolyte mass fraction is essentially the same if those ions are M^+ with OH^- or M^+ with $Fe(CN)_6^{4-}$. For a given pretreatment and counterion, the

https://doi.org/10.1021/acsami.3c14173
ACS Appl. Mater. Interfaces XXXX, XXX, XXX−XXX

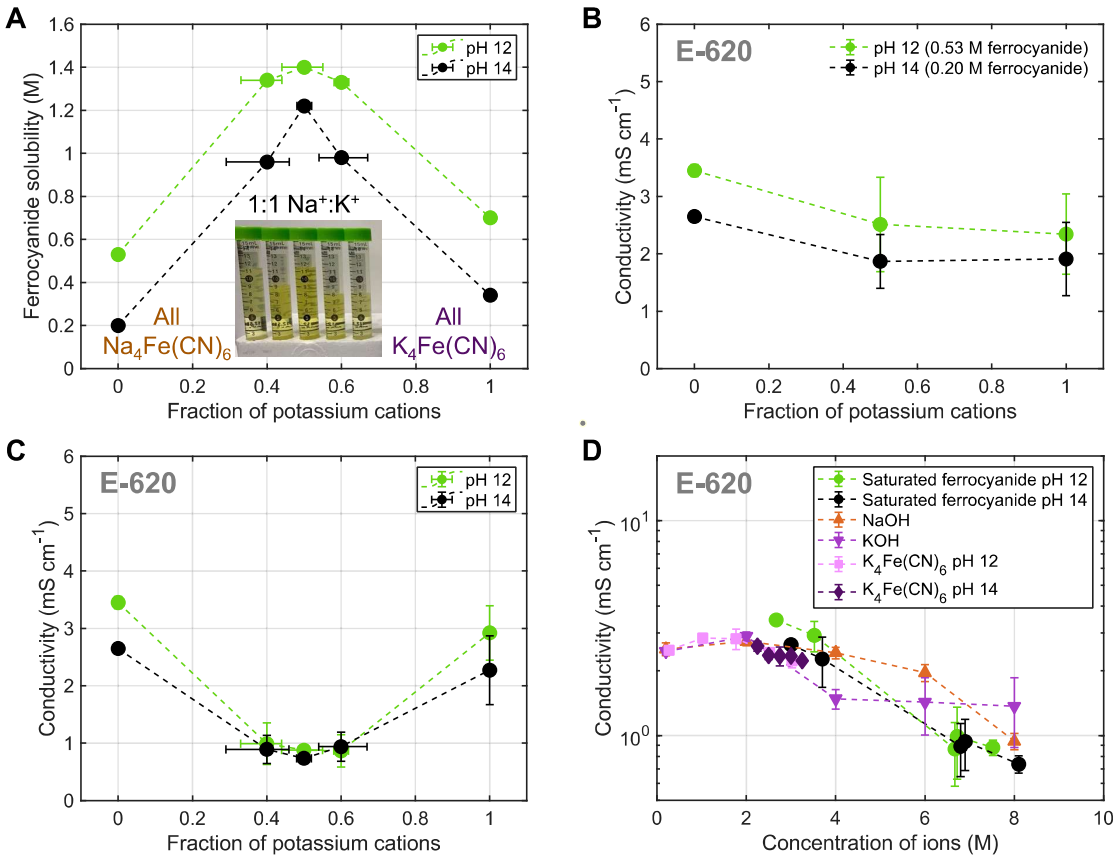

Figure 6. (A) Solubility of ferrocyanide at select ratios of Na^+ and K^+ counterions, with the ordinate ranging from 0 (all Na^+) to 1 (all K^+). (B) Conductivity of E-620 soaked in ferrocyanide flow battery electrolytes with a fixed ferrocyanide concentration (at each pH) but varied ratios of counterions. (C) Conductivity of E-620 soaked in saturated ferrocyanide flow battery electrolytes and select ratios of counterions (concentrations at the solubility limit shown in panel A). (D) Conductivity of E-620 soaked in select electrolytes versus total concentration of ions in the electrolytes (note the semilog scale). Corresponding data for panel D are tabulated in Tables S3, S6, and S7.

effect of adding supporting salt or redox reactant is the same. This result may be generally true when the redox reactant is a co-ion of the ion-exchange membrane (i.e., both anionic or both cationic), which is the case for anionic redox reactants paired with cation-exchange membranes and cationic redox reactants paired with anion-exchange membranes. In these cases, the redox reactant does not compete with the main charge-carrying ion for uptake into the membrane, as is known to occur, for example, with vanadium ions and protons.[63]

Finally, we pushed this membrane−electrolyte system to its limits of ferrocyanide concentration by making use of the diverse ion effect to maximize ferrocyanide solubility with a mix of sodium and potassium counterions.[74−76] The solubility of ferrocyanide with various counterions has received attention in the battery literature due to the relatively low (for a battery electrolyte) solubility of sodium and potassium ferrocyanide salts.[77−80] Although some efforts to boost ferrocyanide solubility with mixed sodium and potassium counterions have been reported, here, we systematically vary the Na^+/K^+ ratio, including for the supporting electrolyte (0.01 or 1 M MOH). Figure 6A shows that the ferrocyanide concentration is maximized at a Na^+/K^+ ratio of 1:1 and that the increased hydroxide concentration decreases ferrocyanide solubility.

We studied E-620 soaked in mixed-cation ferrocyanide solutions in order to isolate the effect of ferrocyanide concentration from cation effects, as we have shown that, unlike Nafion, E-620 does not undergo significant changes in properties when soaked in sodium vs potassium electrolytes. Indeed, Figure 6B shows that for a given ferrocyanide concentration (here, the solubility limit of $Na_4Fe(CN)_6$ in NaOH supporting electrolyte), varying the Na^+/K^+ ratio has only a minor effect on the conductivity of E-620.

Figure 6C shows E-620 conductivity vs fraction of potassium cations for saturated solutions of ferrocyanide in the given supporting electrolytes. The results show that as the 1:1 Na^+/K^+ ratio is approached and the solubility limit is maximized, the conductivity of E-620 drops. The saturated 1:1 Na^+/K^+ electrolyte holds the most ferrocyanide but gives the lowest membrane conductivity, reiterating the trade-off of resistance and volumetric capacity, here, at the extreme of ferrocyanide concentration for this system. Figure 6D shows E-620 conductivity vs total concentration of ions. Unlike the Nafion results shown in Figure 5A, E-620 conductivity is essentially constant or decreasing with ion concentration from 1 M and beyond for both sodium and potassium counterions. E-620 results with MOH supporting electrolyte only, representative potassium ferrocyanide-based battery electrolytes, and saturated mixed counterion ferrocyanide electrolytes are all roughly overlaid, following the same trend with concentration. With the mixed counterion strategy, here, we exceed 8 M total ion concentration with a saturated ferrocyanide-based battery electrolyte.

https://doi.org/10.1021/acsami.3c14173
ACS Appl. Mater. Interfaces XXXX, XXX, XXX−XXX

CONCLUSIONS

The measurements of conductivity, ferricyanide permeability, and electrolyte mass fraction of commercially available cation-exchange membranes soaked in technologically relevant alkaline electrolytes we report here, and the insights synthesized from the results, illustrate our membrane–electrolyte system approach. For the specific system pertinent to alkaline flow batteries, we make the following conclusions:

1. For Nafion N117, cation species and pretreatment strongly affect electrolyte mass fraction and conductivity. We attribute the higher conductivity and higher electrolyte mass fraction of Nafion when sodium-exchanged, compared to potassium-exchanged, to arise from sodium ions bringing more water to form the membrane pores. Pretreatment (20 min soaked in deionized water at 80 °C followed by 35 min soaked in 5% hydrogen peroxide in water at room temperature) also increases conductivity and electrolyte mass fraction.
2. Unlike Nafion, E-620 exhibits similar properties when soaked in sodium and potassium-based electrolytes. This suggests that, unlike Nafion, the polymer E-620 comprises does not undergo significant structural rearrangement upon cation exchange.
3. Pretreated Nafion exhibits high ferricyanide permeability of 10^{-7} to 10^{-8} cm^2 s^{-1}, which is far too high for a practical battery. In contrast, as-received Nafion and E-620 exhibit undetectable crossover, enabling projected decadal lifetimes of flow battery systems.
4. A trade-off between high volumetric capacity and areal power density (from low resistance) arises for high-concentration electrolytes. This trade-off may also arise when, due to cation-dependent active species solubility and membrane resistance, a given cation provides, for example, relatively higher active species solubility but lower conductivity (as is the case with Nafion and potassium ferrocyanide in this study).

Based on these conclusions, we emphasize that due to exceptionally low ferricyanide permeability, the properties of as-received Nafion are important benchmarks to compare against new membranes tailored for flow batteries and should be used to set ambitious targets for the development of flow cells with improved membrane resistance and negligible crossover rates. We also note that the trade-off we identify between volumetric capacity and areal power density in flow batteries may be optimized with careful technoeconomic analysis. The results of such analysis, however, will be highly sensitive to the mass production costs of both membranes and electrolytes, which may not be adequately constrained for conclusions to be drawn at the present time.

Beyond the specific system reported here, our results suggest general principles to consider during the design of membrane–electrolyte systems for diverse electrochemical devices:

1. The qualitative trends of electrolyte conductivity with the composition and concentration do not necessarily match the corresponding conductivity trends for a polymer electrolyte in contact with that solution. The membrane penalty is a dimensionless metric, the ratio of these respective values at a given concentration and composition of the contacting electrolyte that captures the extent to which the presence of a membrane impedes ion transport.
2. Increasing the ion concentration of the contacting electrolyte favors dehydration of the membrane phase, decreasing the electrolyte mass fraction. The electrolyte mass fraction of a given hydrated membrane regulates the influence of ion concentration on conductivity. To a point, increased ion concentration may increase membrane conductivity, but ultimately loss of electrolyte mass fraction may constrain ion transport too severely, decreasing conductivity.

A membrane in contact with the electrolyte in an electrochemical device constitutes a system that is driven toward a two-phase equilibrium. The equilibrium is determined by the composition of the system. We have used this understanding to develop a membrane–electrolyte system approach for performing and interpreting experiments characterizing the ionic conductivity, permeability, and electrolyte mass fraction of membranes. The approach and the insights it provides may benefit the development of an ever-expanding field of electrochemical flow reactors toward widespread electrification of chemistry for a more sustainable future.

ASSOCIATED CONTENT

Supporting Information

The Supporting Information is available free of charge at https://pubs.acs.org/doi/10.1021/acsami.3c14173.

Images of experimental setups; results from crossover measurements; discussion on capacity loss and crossover; tabulated conductivity and electrolyte mass fraction data (PDF)

AUTHOR INFORMATION

Corresponding Author

Michael J. Aziz – *Harvard John A. Paulson School of Engineering and Applied Sciences, Cambridge, Massachusetts 02138, United States;* orcid.org/0000-0001-9657-9456; Email: maziz@harvard.edu

Authors

Thomas Y. George – *Harvard John A. Paulson School of Engineering and Applied Sciences, Cambridge, Massachusetts 02138, United States;* orcid.org/0000-0002-0159-8521

Isabelle C. Thomas – *Harvard John A. Paulson School of Engineering and Applied Sciences, Cambridge, Massachusetts 02138, United States; Emmanuel College, University of Cambridge, Cambridge CB2 1TN, U.K.*

Naphtal O. Haya – *Harvard College, Cambridge, Massachusetts 02138, United States*

John P. Deneen – *Harvard College, Cambridge, Massachusetts 02138, United States*

Cliffton Wang – *Harvard College, Cambridge, Massachusetts 02138, United States*

Complete contact information is available at: https://pubs.acs.org/10.1021/acsami.3c14173

Author Contributions

T.Y.G. conceived the project, developed the methods, and wrote the original draft. T.Y.G., I.C.T., N.O.H., J.P.D., and C.W. performed experiments and analyzed the data. I.C.T. validated the reproducibility of the experimental data. T.Y.G. and M.J.A. supervised the experiments and administrated the

https://doi.org/10.1021/acsami.3c14173
ACS Appl. Mater. Interfaces XXXX, XXX, XXX−XXX

project. M.J.A. acquired funding. All authors reviewed and edited the draft.

Funding

This work was funded in part by U.S. DOE award DE-AC05-76RL01830 through PNNL subcontract 535264. T.Y.G. was supported by the National Science Foundation Graduate Research Fellowship Program under Grant No. DGE 1745303. The Harvard College Program for Research in Science and Engineering (PRISE) supported I.C.T., N.O.H., J.P.D., and C.W.

Notes

The authors declare no competing financial interest.

■ ACKNOWLEDGMENTS

The information, data, or work presented herein was funded in part by U.S. DOE award DE-AC05-76RL01830 through PNNL subcontract 535264. This material is based upon work supported by the National Science Foundation Graduate Research Fellowship Program under Grant No. DGE 1745303 (supporting T.Y.G.). Any opinions, findings, and conclusions or recommendations expressed in this material are those of the authors and do not necessarily reflect the views of the National Science Foundation. The authors also acknowledge support from the Harvard College Program for Research in Science and Engineering (PRISE), supporting I.C.T., N.O.H., J.P.D., and C.W. They acknowledge Dr. Bernd Bauer of Fumatech for providing Fumasep E-620 membranes free of charge. They also acknowledge Prof. Fikile Brushett and his research group for providing the Gen. 2 flow cell. Finally, they acknowledge Eric Fell for insightful discussions on the membrane penalty.

■ REFERENCES

(1) Davis, S. J.; Lewis, N. S.; Shaner, M.; Aggarwal, S.; Arent, D.; Azevedo, I. L.; Benson, S. M.; Bradley, T.; Brouwer, J.; Chiang, Y. M.; Clack, C. T.; Cohen, A.; Doig, S.; Edmonds, J.; Fennell, P.; Field, C. B.; Hannegan, B.; Hodge, B. M.; Hoffert, M. I.; Ingersoll, E.; Jaramillo, P.; Lackner, K. S.; Mach, K. J.; Mastrandrea, M.; Ogden, J.; Peterson, P. F.; Sanchez, D. L.; Sperling, D.; Stagner, J.; Trancik, J. E.; Yang, C. J.; Caldeira, K. Net-zero Emissions Energy Systems. *Science* **2018**, *360*, No. eaas9793.

(2) Kusoglu, A.; Weber, A. Z. New Insights into Perfluorinated Sulfonic-Acid Ionomers. *Chem. Rev.* **2017**, *117*, 987−1104.

(3) Weber, A. Z.; Mench, M. M.; Meyers, J. P.; Ross, P. N.; Gostick, J. T.; Liu, Q. Redox Flow Batteries: A Review. *J. Appl. Electrochem.* **2011**, *41*, 1137−1164.

(4) Tolmachev, Y. V. Review—Flow Batteries from 1879 to 2022 and Beyond. *J. Electrochem. Soc.* **2023**, *170*, No. 030505.

(5) Chen, Q.; Saal, Y.; Yuan, Z.; Li, X.; Yu, G.; Yang, Z.; Xu, T. Organic Electrolytes for pH-Neutral Aqueous Organic Redox Flow Batteries. *Adv. Funct. Mater.* **2021**, *32* (9), No. 2108777, DOI: 10.1002/adfm.202108777.

(6) Li, Z.; Jiang, T.; Ali, M.; Wu, C.; Chen, W. Recent Progress in Organic Species for Redox Flow Batteries. *Energy Storage Mater.* **2022**, *50*, 105−138.

(7) Cannon, C. G.; Klusener, P. A. A.; Brandon, N. P.; Kucernak, A. Aqueous Redox Flow Batteries: Small Organic Molecules for the Positive Electrolyte Species. *ChemSusChem* **2023**, *16*, No. e202300303.

(8) Weiss, T. A.; Fan, G.; Neyhouse, B. J.; Moore, E. B.; Furst, A.; Brushett, F. R. Characterizing the Impact of Oligomerization on Redox Flow Cell Performance. *Batteries Supercaps* **2023**, *6*, No. e202300034.

(9) Lv, X.-L.; Sullivan, P. T.; Li, W.; Fu, H.-C.; Jacobs, R.; Chen, C.-J.; Morgan, D.; Jin, S.; Feng, D. Modular Dimerization of Organic Radicals for Stable and Dense Flow Battery Catholyte. *Nat. Energy* **2023**, *8*, 1109−1118.

(10) Saal, A.; Hagemann, T.; Schubert, U. S. Polymers for Battery Applications—Active Materials, Membranes, and Binders. *Adv. Energy Mater.* **2021**, *11*, No. 2001984.

(11) Robb, B. H.; Farrell, J. M.; Marshak, M. P. Chelated Chromium Electrolyte Enabling High-Voltage Aqueous Flow Batteries. *Joule* **2019**, *3*, 2503−2512.

(12) Waters, S. E.; Robb, B. H.; Marshak, M. P. Effect of Chelation on Iron-Chromium Redox Flow Batteries. *ACS Energy Lett.* **2020**, *5*, 1758−1762.

(13) Ruan, W.; Mao, J.; Yang, S.; Chen, Q. Communication-Tris(bipyridyl)iron Complexes for High-Voltage Aqueous Redox Flow Batteries. *J. Electrochem. Soc.* **2020**, *167*, No. 100543.

(14) Gao, J.; Amini, K.; George, T. Y.; Jing, Y.; Tsukamoto, T.; Xi, D.; Gordon, R. G.; Aziz, M. J. A High Potential, Low Capacity Fade Rate Iron Complex Posolyte for Aqueous Organic Flow Batteries. *Adv. Energy Mater.* **2022**, *12*, No. 2202444.

(15) Liu, Y.; Zhang, J.; Lu, S.; Xiang, Y. Polyoxometalate-Based Electrolyte Materials in Redox Flow Batteries: Current Trends and Emerging Opportunities. *Mater. Rep.: Energy* **2022**, *2*, 100094.

(16) Fell, E. M.; De Porcellinis, D.; Jing, Y.; Gutierrez-Venegas, V.; George, T. Y.; Gordon, R. G.; Granados-Focil, S.; Aziz, M. J. Long-Term Stability of Ferri-Ferrocyanide as an Electroactive Component for Redox Flow Battery Applications: On the Origin of Apparent Capacity Fade. *J. Electrochem. Soc.* **2023**, *170*, No. 070525.

(17) Jang, J.-E.; ah Kim, R.; Jayasubramaniyan, S.; Lee, C.; Choi, J.; Lee, Y.; Kang, S.; Ryu, J.; Lee, S. W.; Cho, J.; Lee, D. W.; Song, H.-K.; Choe, W.; Seo, D.-H.; Lee, H.-W. Full-Hexacyanometallate Aqueous Redox Flow Batteries Exceeding 1.5 V in an Aqueous Solution. *Adv. Energy Mater.* **2023**, *13*, No. 2300707.

(18) Jing, Y.; Wu, M.; Wong, A. A.; Fell, E. M.; Jin, S.; Pollack, D. A.; Kerr, E. F.; Gordon, R. G.; Aziz, M. J. In Situ Electrosynthesis of Anthraquinone Electrolytes in Aqueous Flow Batteries. *Green Chem.* **2020**, *22*, 6084.

(19) Adewuyi, A.; Akinrele, J. Design and Construction of Redox Flow Battery using Liquid Extract from Morinda Lucida Leaves. *J. Appl. Sci. Environ. Manage.* **2022**, *26*, 187−190.

(20) Kwabi, D. G.; Ji, Y.; Aziz, M. J. Electrolyte Lifetime in Aqueous Organic Redox Flow Batteries: A Critical Review. *Chem. Rev.* **2020**, *120*, 6467−6489.

(21) Kwabi, D. G.; Lin, K.; Ji, Y.; Kerr, E. F.; Goulet, M. A.; De Porcellinis, D.; Tabor, D. P.; Pollack, D. A.; Aspuru-Guzik, A.; Gordon, R. G.; Aziz, M. J. Alkaline Quinone Flow Battery with Long Lifetime at pH 12. *Joule* **2018**, *2*, 1894−1906.

(22) Ji, Y.; Goulet, M. A.; Pollack, D. A.; Kwabi, D. G.; Jin, S.; De Porcellinis, D.; Kerr, E. F.; Gordon, R. G.; Aziz, M. J. A Phosphonate-Functionalized Quinone Redox Flow Battery at Near-Neutral pH with Record Capacity Retention Rate. *Adv. Energy Mater.* **2019**, *9*, No. 1900039.

(23) Wu, M.; Jing, Y.; Wong, A. A.; Fell, E. M.; Jin, S.; Tang, Z.; Gordon, R. G.; Aziz, M. J. Extremely Stable Anthraquinone Negolytes Synthesized from Common Precursors. *Chem* **2020**, *6*, 1432−1442.

(24) Pang, S.; Wang, X.; Wang, P.; Ji, Y. Biomimetic Amino Acid Functionalized Phenazine Flow Batteries with Long Lifetime at Near-Neutral pH. *Angew. Chem., Int. Ed.* **2021**, *60*, 5289−5298.

(25) Xu, J.; Pang, S.; Wang, X.; Wang, P.; Ji, Y. Ultrastable Aqueous Phenazine Flow Batteries with High Capacity Operated at Elevated Temperatures. *Joule* **2021**, *5*, 2437−2449.

(26) Jing, Y.; Fell, E. M.; Wu, M.; Jin, S.; Ji, Y.; Pollack, D. A.; Tang, Z.; Ding, D.; Bahari, M.; Goulet, M.-A.; Tsukamoto, T.; Gordon, R. G.; Aziz, M. J. Anthraquinone Flow Battery Reactants with Nonhydrolyzable Water-Solubilizing Chains Introduced via a Generic Cross-Coupling Method. *ACS Energy Lett.* **2022**, *7*, 226−235.

(27) Crothers, A. R.; Darling, R. M.; Kusoglu, A.; Radke, C. J.; Weber, A. Z. Theory of Multicomponent Phenomena in Cation-Exchange Membranes: Part I. Thermodynamic Model and Validation. *J. Electrochem. Soc.* **2020**, *167*, 013547.

https://doi.org/10.1021/acsami.3c14173
ACS Appl. Mater. Interfaces XXXX, XXX, XXX−XXX

(28) Crothers, A. R.; Darling, R. M.; Kusoglu, A.; Radke, C. J.; Weber, A. Z. Theory of Multicomponent Phenomena in Cation-Exchange Membranes: Part II. Transport Model and Validation. *J. Electrochem. Soc.* **2020**, *167*, 013548.
(29) Crothers, A. R.; Kusoglu, A.; Radke, C. J.; Weber, A. Z. Influence of Mesoscale Interactions on Proton, Water, and Electro-kinetic Transport in Solvent-Filled Membranes: Theory and Simulation. *Langmuir* **2022**, *38*, 10362−10374.
(30) Darling, R.; Gallagher, K.; Xie, W.; Su, L.; Brushett, F. Transport Property Requirements for Flow Battery Separators. *J. Electrochem. Soc.* **2016**, *163*, A5029−A5040.
(31) Kushner, D. I.; Crothers, A. R.; Kusoglu, A.; Weber, A. Z. Transport Phenomena in Flow Battery Ion-conducting Membranes. *Curr. Opin. Electrochem.* **2020**, *21*, 132−139.
(32) Wu, M.; Bahari, M.; Fell, E. M.; Gordon, R. G.; Aziz, M. J. High-performance Anthraquinone with Potentially Low Cost for Aqueous Redox Flow Batteries. *J. Mater. Chem. A* **2021**, *9*, 26709−26716.
(33) Wu, M.; Bahari, M.; Jing, Y.; Amini, K.; Fell, E. M.; George, T. Y.; Gordon, R. G.; Aziz, M. J. Highly Stable, Low Redox Potential Quinone for Aqueous Flow Batteries. *Batteries Supercaps* **2022**, *5*, No. e202200009.
(34) Amini, K.; Kerr, E. F.; George, T. Y.; Alfaraidi, A. M.; Jing, Y.; Tsukamoto, T.; Gordon, R. G.; Aziz, M. J. An Extremely Stable, Highly Soluble Monosubstituted Anthraquinone for Aqueous Redox Flow Batteries. *Adv. Funct. Mater.* **2023**, *33*, No. 2211338.
(35) Robb, B. H.; Waters, S. E.; Saraidaridis, J. D.; Marshak, M. P. Realized Potential as Neutral pH Flow Batteries Achieve High Power Densities. *Cell Rep. Phys. Sci.* **2022**, *3*, 101118.
(36) Huskinson, B.; Rugolo, J.; Mondal, S. K.; Aziz, M. J. A High Power Density, High Efficiency Hydrogen-Chlorine Regenerative Fuel Cell with a Low Precious Metal Content Catalyst. *Energy Environ. Sci.* **2012**, *5*, 8690−8698.
(37) Huskinson, B.; Marshak, M. P.; Suh, C.; Er, S.; Gerhardt, M. R.; Galvin, C. J.; Chen, X.; Aspuru-Guzik, A.; Gordon, R. G.; Aziz, M. J. A Metal-free Organic-inorganic Aqueous Flow Battery. *Nature* **2014**, *505*, 195−198.
(38) Lin, K.; Chen, Q.; Gerhardt, M. R.; Tong, L.; Kim, S. B.; Eisenach, L.; Valle, A. W.; Hardee, D.; Gordon, R. G.; Aziz, M. J.; Marshak, M. P. Alkaline Quinone Flow Battery. *Science* **2015**, *349*, 1529−1532.
(39) De Porcellinis, D.; Mecheri, B.; D'Epifanio, A.; Licoccia, S.; Granados-Focil, S.; Aziz, M. J. Communication−Sulfonated Poly (ether ether ketone) as Cation Exchange Membrane for Alkaline Redox Flow Batteries. *J. Electrochem. Soc.* **2018**, *165*, A1137−A1139.
(40) Baran, M. J.; Braten, M. N.; Sahu, S.; Baskin, A.; Meckler, S. M.; Li, L.; Maserati, L.; Carrington, M. E.; Chiang, Y.-M.; Prendergast, D.; Helms, B. A. Design Rules for Membranes from Polymers of Intrinsic Microporosity for Crossover-free Aqueous Electrochemical Devices. *Joule* **2019**, *3*, 2968−2985.
(41) Tan, R.; Wang, A.; Malpass-Evans, R.; Williams, R.; Zhao, E. W.; Liu, T.; Ye, C.; Zhou, X.; Darwich, B. P.; Fan, Z.; Turcani, L.; Jackson, E.; Chen, L.; Chong, S. Y.; Li, T.; Jelfs, K. E.; Cooper, A. I.; Brandon, N. P.; Grey, C. P.; Mckeown, N. B.; Song, Q. Hydrophilic Microporous Membranes for Selective Ion Separation and Flow-Battery Energy Storage. *Nat. Mater.* **2020**, *19*, 195−202.
(42) Zuo, P.; Li, Y.; Wang, A.; Tan, R.; Liu, Y.; Liang, X.; Sheng, F.; Tang, G.; Ge, L.; Wu, L.; Song, Q.; McKeown, N. B.; Yang, Z.; Xu, T. Sulfonated Microporous Polymer Membranes with Fast and Selective Ion Transport for Electrochemical Energy Conversion and Storage. *Angew. Chem., Int. Ed.* **2020**, *59*, 9564−9573.
(43) Xia, Y.; Cao, H.; Xu, F.; Chen, Y.; Xia, Y.; Zhang, D.; Dai, L.; Qu, K.; Lian, C.; Huang, K.; Xing, W.; Jin, W.; Xu, Z. Polymeric Membranes with Aligned Zeolite Nanosheets for Sustainable Energy Storage. *Nat. Sustainability* **2022**, *5*, 1080−1091.
(44) Ye, C.; Wang, A.; Breakwell, C.; Tan, R.; Bezzu, C. G.; Hunter-Sellars, E.; Williams, D. R.; Brandon, N. P.; Klusener, P. A.; Kucernak, A. R.; Jelfs, K. E.; McKeown, N. B.; Song, Q. Development of Efficient Aqueous Organic Redox Flow Batteries Using Ion-sieving Sulfonated Polymer Membranes. *Nat. Commun.* **2022**, *13*, No. 3184.
(45) Ye, C.; Tan, R.; Wang, A.; Chen, J.; Gándara, B. C.; Breakwell, C.; Alvarez-Fernandez, A.; Fan, Z.; Weng, J.; Bezzu, C. G.; Guldin, S.; Brandon, N. P.; Kucernak, A. R.; Jelfs, K. E.; McKeown, N. B.; Song, Q. Long-Life Aqueous Organic Redox Flow Batteries Enabled by Amidoxime-Functionalized Ion-Selective Polymer Membranes. *Angew. Chem., Int. Ed.* **2022**, *61*, No. e202207580.
(46) Wang, A.; Tan, R.; Liu, D.; Lu, J.; Wei, X.; Alvarez-Fernandez, A.; Ye, C.; Breakwell, C.; Guldin, S.; Kucernak, A. P.; Jelfs, K. E.; Brandon, N. P.; McKeown, N. B.; Song, Q. Ion-selective Microporous Polymer Membranes with Hydrogen-bond and Salt-bridge Networks for Aqueous Organic Redox Flow Batteries. *Adv. Mater.* **2023**, *35*, No. 2210098.
(47) Tan, R.; Wang, A.; Ye, C.; Li, J.; Liu, D.; Darwich, B. P.; Petit, L.; Fan, Z.; Wong, T.; Alberto, A.-F.; Furedi, M.; Guldin, S.; Breakwell, C. E.; Klusener, P. A. A.; Kucernak, A. R.; Jelfs, K. E.; McKeown, N. B.; Song, Q. Thin Film Composite Membranes with Regulated Crossover and Water Migration for Long-Life Aqueous Redox Flow Batteries. *Adv. Sci.* **2023**, *10*, No. 2206888.
(48) Zuo, P.; Ye, C.; Jiao, Z.; Luo, J.; Fang, J.; Schubert, U. S.; McKeown, N. B.; Liu, T. L.; Yang, Z.; Xu, T. Near-frictionless Ion Transport Within Triazine Framework Membranes. *Nature* **2023**, *617*, 299−305.
(49) Arellano, C. A. P.; Martínez, S. S. Effects of pH on the Degradation of Aqueous Ferricyanide by Photolysis and Photo-catalysis under Solar Radiation. *Sol. Energy Mater. Sol. Cells* **2010**, *94*, 327−332.
(50) Robb, B. H.; George, T. Y.; Davis, C. M.; Tang, Z.; Fujimoto, C. H.; Aziz, M. J.; Marshak, M. P. Sulfonated Diels-Alder Poly(phenylene) Membrane for Efficient Ion-Selective Transport in Aqueous Metalorganic and Organic Redox Flow Batteries. *J. Electrochem. Soc.* **2023**, *170*, No. 030515.
(51) George, T. Y.; Kerr, E. F.; Haya, N. O.; Alfaraidi, A. M.; Gordon, R. G.; Aziz, M. J. Size and Charge Effects on Crossover of Flow Battery Reactants Evaluated by Quinone Permeabilities Through Nafion. *J. Electrochem. Soc.* **2023**, *170*, 040509.
(52) Yang, Z.; Tong, L.; Tabor, D. P.; Goulet, M.-A.; De Porcellinis, D.; Aspuru-Guzik, A.; Gordon, R. G.; Aziz, M. J. Alkaline Benzoquinone Aqueous Flow Battery for Large-Scale Storage of Electrical Energy. *Adv. Energy Mater.* **2017**, *8* (8), No. 1702056.
(53) Xie, W.; Darling, R. M.; Perry, M. L. Processing and Pretreatment Effects on Vanadium Transport in Nafion Membranes. *J. Electrochem. Soc.* **2016**, *163*, A5084−A5089.
(54) Jiang, B.; Wu, L.; Yu, L.; et al. A Comparative Study of Nafion Series Membranes for Vanadium Redox Flow Batteries. *J. Membr. Sci.* **2016**, *510*, 18−26.
(55) Tang, Z.; Svoboda, R.; Lawton, J. S.; Aaron, D. S.; Papandrew, A. B.; Zawodzinski, T. A. Composition and Conductivity of Membranes Equilibrated with Solutions of Sulfuric Acid and Vanadyl Sulfate. *J. Electrochem. Soc.* **2013**, *160*, F1040−F1047.
(56) Pintauro, P. N.; Bennion, D. N. Mass transport of electrolytes in membranes. 2. Determination of sodium chloride equilibrium and transport parameters for Nafion. *Ind. Eng. Chem. Fundam.* **1984**, *23*, 234−243.
(57) Stenina, I. A.; Sistat, P.; Rebrov, A. I.; Pourcelly, G.; Yaroslavtsev, A. B. Ion mobility in Nafion-117 membranes. *Desalination* **2004**, *170*, 49−57.
(58) Tong, L.; Goulet, M. A.; Tabor, D. P.; Kerr, E. F.; De Porcellinis, D.; Fell, E. M.; Aspuru-Guzik, A.; Gordon, R. G.; Aziz, M. J. Molecular Engineering of an Alkaline Naphthoquinone Flow Battery. *ACS Energy Lett.* **2019**, *4*, 1880−1887.
(59) Jin, S.; Fell, E. M.; Vina-Lopez, L.; Jing, Y.; Michalak, P. W.; Gordon, R. G.; Aziz, M. J. Near Neutral pH Redox Flow Battery with Low Permeability and Long-Lifetime Phosphonated Viologen Active Species. *Adv. Energy Mater.* **2020**, *10*, No. 2000100.
(60) Gierke, T. D.; Munn, G. E.; Wilson, F. C. The Morphology in Nafion* Perfluorinated Membrane Products, as Determined by Wide-

https://doi.org/10.1021/acsami.3c14173
ACS Appl. Mater. Interfaces XXXX, XXX, XXX−XXX

and Small-Angle X-Ray Studies. *J. Polym. Sci., Polym. Phys. Ed.* **1981**, *19*, 1687−1704.
(61) Shi, S.; Weber, A. Z.; Kusoglu, A. Structure-transport Relationship of Perfluorosulfonic-acid membranes in Different Cationic Forms. *Electrochim. Acta* **2016**, *220*, 517−528.
(62) Rollet, A.-L.; Gebel, G.; Simonin, J.-P.; Turq, P. A SANS Determination of the Influence of External Conditions on the Nanostructure of Nafion Membrane. *J. Polym. Sci., Part B: Polym. Phys.* **2001**, *39*, 548−558.
(63) Elgammal, R. A.; Tang, Z.; Sun, C. N.; Lawton, J.; Zawodzinski, T. A. Species Uptake and Mass Transport in Membranes for Vanadium Redox Flow Batteries. *Electrochim. Acta* **2017**, *237*, 1−11.
(64) Gering, K. L. Prediction of Electrolyte Viscosity for Aqueous and Non-aqueous Systems: Results from a Molecular Model Based on Ion Solvation and a Chemical Physics Framework. *Electrochim. Acta* **2006**, *51*, 3125−3138.
(65) Gering, K. L. Prediction of Electrolyte Conductivity: Results from a Generalized Molecular Model Based on Ion Solvation and a Chemical Physics Framework. *Electrochim. Acta* **2017**, *225*, 175−189.
(66) See, D. M.; White, R. E. Temperature and Concentration Dependence of the Specific Conductivity of Concentrated Solutions of Potassium Hydroxide. *J. Chem. Eng. Data* **1997**, *42*, 1266−1268.
(67) Gilliam, R. J.; Graydon, J. W.; Kirk, D. W.; Thorpe, S. J. A Review of Specific Conductivities of Potassium Hydroxide Solutions for Various Concentrations and Temperatures. *Int. J. Hydrogen Energy* **2007**, *32*, 359−364.
(68) Doris, S. E.; Ward, A. L.; Baskin, A.; Frischmann, P. D.; Gavvalapalli, N.; Chénard, E.; Sevov, C. S.; Prendergast, D.; Moore, J. S.; Helms, B. A. Macromolecular Design Strategies for Preventing Active-Material Crossover in Non-Aqueous All-Organic Redox-Flow Batteries. *Angew. Chem.* **2017**, *129*, 1617−1621.
(69) Hendriks, K. H.; Robinson, S. G.; Braten, M. N.; Sevov, C. S.; Helms, B. A.; Sigman, M. S.; Minteer, S. D.; Sanford, M. S. High-Performance Oligomeric Catholytes for Effective Macromolecular Separation in Nonaqueous Redox Flow Batteries. *ACS Cent. Sci.* **2018**, *4*, 189−196.
(70) Van Zee, J.; White, R. E. Using Parameter Estimation Techniques with a Simple Model of a Diaphragm-Type Electrolyzer to Predict the Electrical Energy Cost for NaOH Production. *J. Electrochem. Soc.* **1985**, *132*, 818−826.
(71) Kyi, A. A.; Batchelor, B. An Electrical Conductivity Method for Measuring the Effects of Additives on Effective Diffusivities in Portland Cement Pastes. *Cement Concr. Res.* **1994**, *24*, 752−764.
(72) Zhang, S. S. A Review on the Separators of Liquid Electrolyte Li-ion Batteries. *J. Power Sources* **2007**, *164*, 351−364.
(73) DuBeshter, T.; Sinha, P. K.; Sakars, A.; Fly, G. W.; Jornea, J. Measurement of Tortuosity and Porosity of Porous Battery Electrodes. *J. Electrochem. Soc.* **2014**, *161*, A599−A605.
(74) Trant, C.; Vercillo, P. *Solubility of Sodium Ferrocyanide and Potassium Ferrocyanide in Solutions of NaOH and KOH Mixtures at 25 °C*; University of Rochester, 2011.
(75) Esswein, A. J.; Goeltz, J.; Amadeo, D. High Solubility Iron Hexacyanides. US11349141B2, 2022.
(76) Wang, G.; Zou, H.; Xu, Z.; Tang, A.; Zhong, F.; Zhu, X.; Qin, C.; Ding, M.; You, W.; Jia, C. Unlocking the Solubility Limit of Ferrocyanide for High Energy Density Redox Flow Batteries. *Mater. Today Energy* **2022**, *28*, 101061.
(77) Luo, J.; Hu, B.; Debruler, C.; Bi, Y.; Zhao, Y.; Yuan, B.; Hu, M.; Wu, W.; Liu, T. L. Unprecedented Capacity and Stability of Ammonium Ferrocyanide Catholyte in pH Neutral Aqueous Redox Flow Batteries. *Joule* **2019**, *3*, 149−163.
(78) Waters, S. E.; Thurston, J. R.; Armstrong, R. W.; Robb, B. H.; Marshak, M. P.; Reber, D. Holistic Design Principles for Flow Batteries: Cation Dependent Membrane Resistance and Active Species Solubility. *J. Power Sources* **2022**, *520*, 230877.
(79) Reber, D.; Thurston, J. R.; Becker, M.; Marshak, M. P. Stability of Highly Soluble Ferrocyanides at Neutral pH for Energy-dense Flow Batteries. *Cell Rep. Phys. Sci.* **2023**, *4*, 101215.
(80) Li, X.; Yao, Y.; Liu, C.; Jia, X.; Jian, J.; Guo, B.; Lu, S.; Qin, W.; Wang, Q.; Wu, X. Lithium Ferrocyanide Catholyte for High-Energy and Low-cost Aqueous Redox Flow Batteries**. *Angew. Chem., Int. Ed.* **2023**, *62* (25), No. e202304667.

https://doi.org/10.1021/acsami.3c14173
ACS Appl. Mater. Interfaces XXXX, XXX, XXX−XXX

Supporting Information

A Membrane-Electrolyte System Approach to Understanding Ionic Conductivity and Crossover in Alkaline Flow Cells

Thomas Y. George,[†] Isabelle C. Thomas,[†,‡] Naphtal O. Haya,[¶] John P. Deneen,[¶] Cliffton Wang,[¶] and Michael J. Aziz[*,†]

[†]*Harvard John A. Paulson School of Engineering and Applied Sciences, Cambridge, Massachusetts 02138, USA*

[‡]*Emmanuel College, University of Cambridge, Cambridge CB2 1TN, UK*

[¶]*Harvard College, Cambridge, Massachusetts 02138, USA*

E-mail: maziz@harvard.edu

Table of Contents

Figure S1: Photograph of the flow cell hardware used for determining membrane conductivity, showing plastic end plates, manifolds, graphite interdigitated flow fields, gaskets (2.55 cm^2 windows), and Sigracet GDL 39AA electrodes.

Figure S2: Photograph of assembled flow cell with electrolyte circulated on both sides from a single reservoir, using a Masterflex peristaltic pump. The clips connect the cell to a Gamry Reference 3000 potentiostat.

Figure S3: Photograph of example filter paper used to filter precipitates from a saturated solution of ferrocyanide with mixed sodium and potassium counterions and then dried in air. The mass of the precipitates was used to determine horizontal error bars in Figure 6 of the main text.

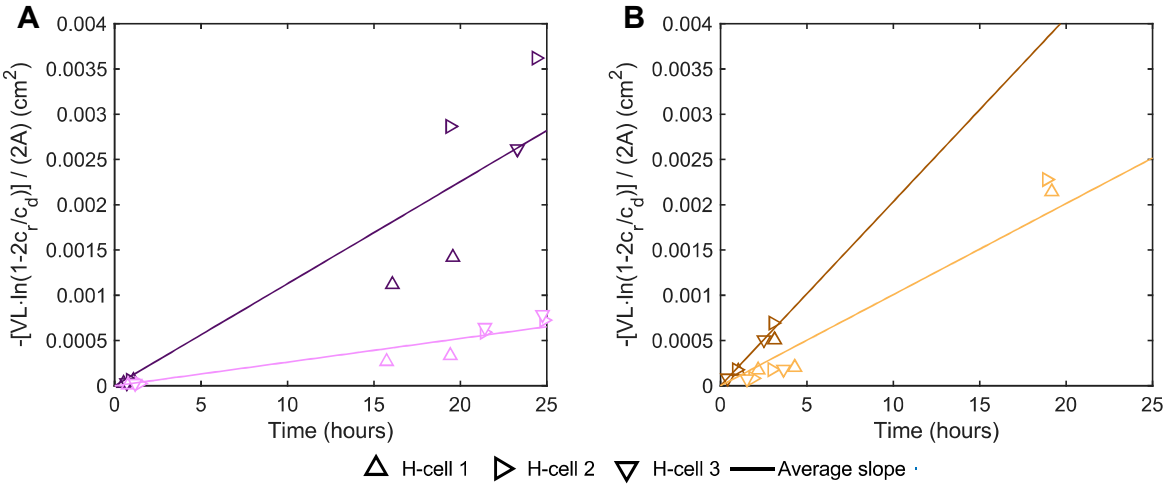

Figure S4: Permeability plots for (a) pre-treated potassium-exchanged NR212 and (b) pre-treated sodium-exchanged NR212, where the slope gives the permeability, based on a formula derived from Fick's Law.[1] V is the electrolyte volume of each side (10 mL), L is the membrane thickness (50 μm), A is the membrane area (1.979 cm^2), $c_r(t)$ is the time-dependent concentration of crossed-over species, and $c_d(0)$ is the concentration of crossing species in the donating electrolyte at start of the experiment (0.2 M or 0.6 M). The slopes of the solid lines are the averages of the three slopes for triplicate H-cells per experimental condition.

Table S1: Permeability data for pre-treated NR212 broken down by measurements from each H-cell as well as reported as the average of triplicate H-cells for each donor electrolyte.

Donor electrolyte (all pH 12)	Permeability from average of three H-cells ($cm^2\ s^{-1}$)	Permeability from each H-cell ($cm^2\ s^{-1}$)	R^2 from determining permeability for each H-cell
0.6 M $Na_3Fe(CN)_6$	$5.6 \times 10^{-8} \pm 9.1 \times 10^{-9}$	4.6×10^{-8}	1 (two points)
		6.8×10^{-8}	1 (two points)
		5.6×10^{-8}	1 (two points)
0.2 M $Na_3Fe(CN)_6$	$2.8 \times 10^{-8} \pm 1.0 \times 10^{-9}$	3.4×10^{-8}	0.990 (three points)
		3.6×10^{-8}	1.000 (three points)
		1.4×10^{-8}	1 (two points)
0.6 M $K_3Fe(CN)_6$	$3.1 \times 10^{-8} \pm 9.0 \times 10^{-9}$	2.0×10^{-8}	1.000 (three points)
		4.2×10^{-8}	1.000 (three points)
		3.2×10^{-8}	1 (two points)
0.2 M $K_3Fe(CN)_6$	$7.3 \times 10^{-9} \pm 1.7 \times 10^{-9}$	4.8×10^{-9}	1.000 (three points)
		8.2×10^{-9}	0.998 (three points)
		8.8×10^{-9}	0.998 (three points)

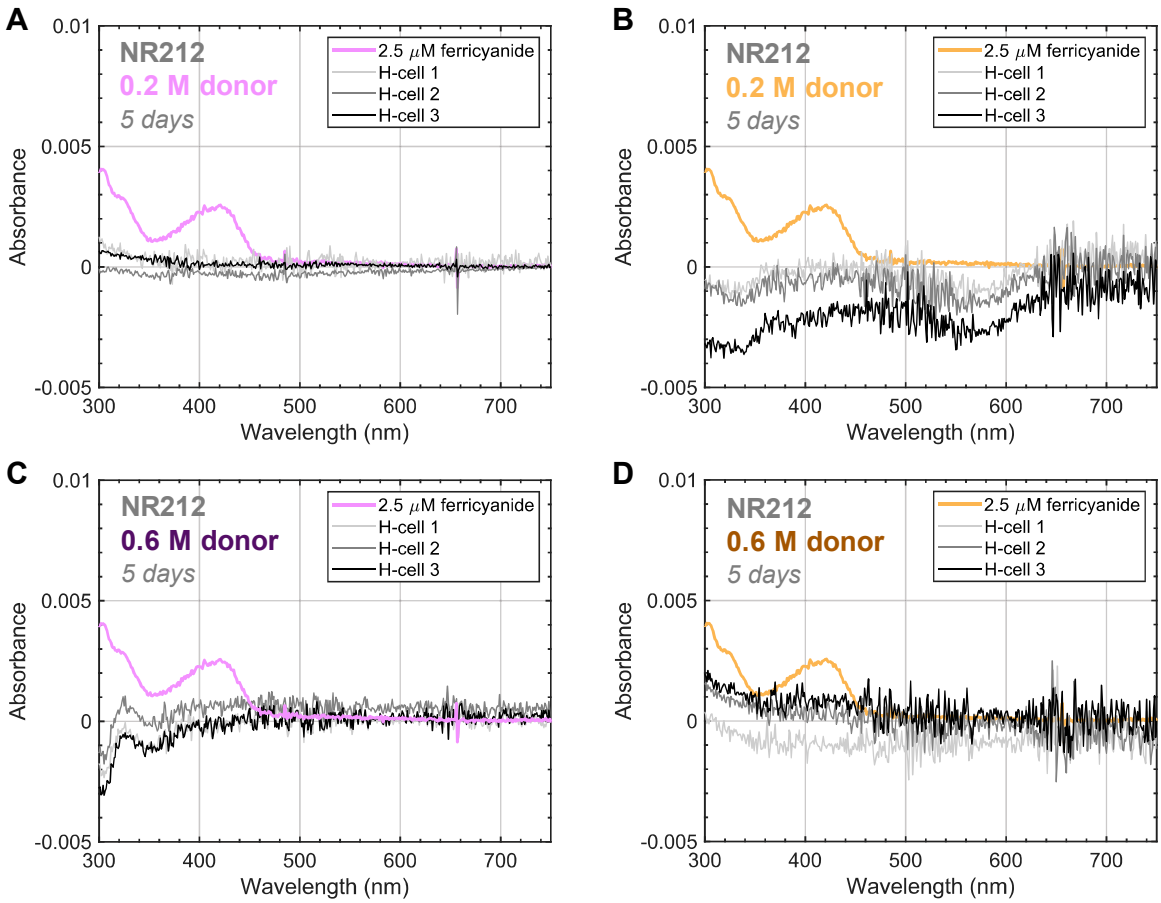

Figure S5: UV-vis absorbance spectra of undiluted H-cell receiving electrolytes after five day experiments for triplicate H-cells comprising as-received potassium- (a,c) or sodium-exchanged (b,d) NR212 and 0.2 M (a,b) or 0.6 M (c,d) donor concentration of ferricyanide. The absorbance spectra show signal beneath the detection limit for ferricyanide at 420 nm (corresponding to 1 μM), indicating undetectable crossover. Absorbance spectra for 2.5 μM potassium ferricyanide from a previously established calibration curve[2] are included for a visual guide.

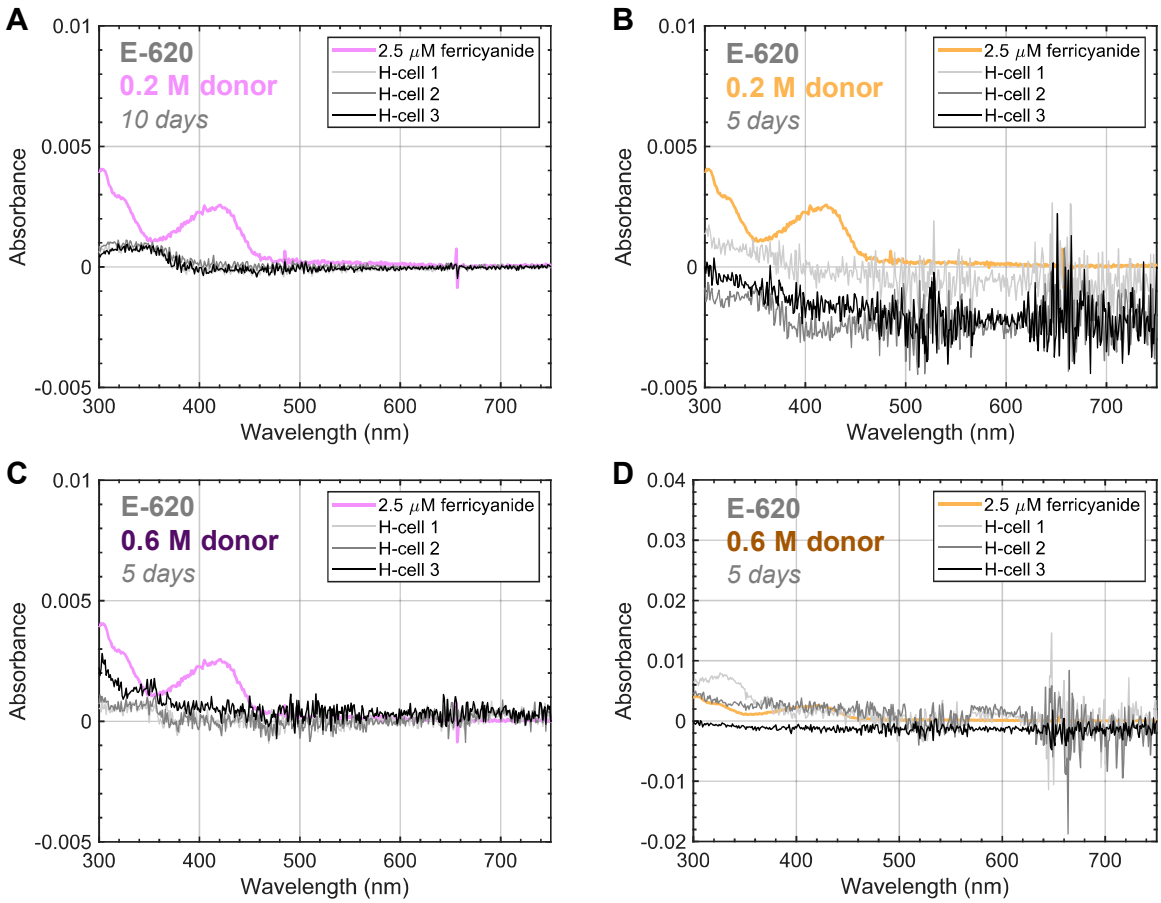

Figure S6: UV-vis absorbance spectra of undiluted H-cell receiving electrolytes after five or ten day (as specified) experiments for triplicate H-cells comprising as-received E-620, 0.2 M (a,b) or 0.6 M (c,d) donor concentration of ferricyanide, with either potassium- (a,c) or sodium-based (b,d) electrolytes. The absorbance spectra in (a-c) show signal beneath the detection limit for ferricyanide at 420 nm (corresponding to 1 μM), indicating undetectable crossover. The absorbance spectra in (d) are noisier than in (a-c) - note zoomed-out y axis to show all of the data - but no clear peak is observed at 420 nm and all absorbance values at 420 nm in this figure fall below the value corresponding to 2.5 μM ferricyanide from a calibration curve. See Note S1 for further discussion of the upper limit of ferricyanide permeability through E-620. Absorbance spectra for 2.5 μM potassium ferricyanide from a previously established calibration curve[2] are included for a visual guide.

Supplementary Discussion 1 - E-620 crossover

Based on the results reported in Figure S6, upper limits on ferricyanide permeability through E-620 may be assigned. These upper limits depend on experiment duration, membrane thick-

ness, and donor concentration, thus we emphasize that a lower reported detection limit does not necessarily mean a lower actual permeability of the membrane. The ten day experiment shown in Figure S6a allows us to report an upper permeability limit of 6×10^{-14} cm^2 s^{-1} with 0.2 M potassium ferricyanide in the donor. Crossover was also undetectable after a 5 day experiment with 0.6 M potassium ferricyanide in the donor, giving an upper permeability limit of 4×10^{-14} cm^2 s^{-1}. With 0.2 M sodium ferricyanide in the donor and a five day experiment, the upper permeability limit is 1×10^{-13} cm^2 s^{-1}. Finally, although the spectra are noisier in Figure S6d, using the highest measured absorbance at 420 nm among the three triplicate H-cells gives a permeability value of 2×10^{-13} cm^2 s^{-1}. All of these permeability values are low enough to enable extremely stable flow battery capacity under typical lab scale experiments.

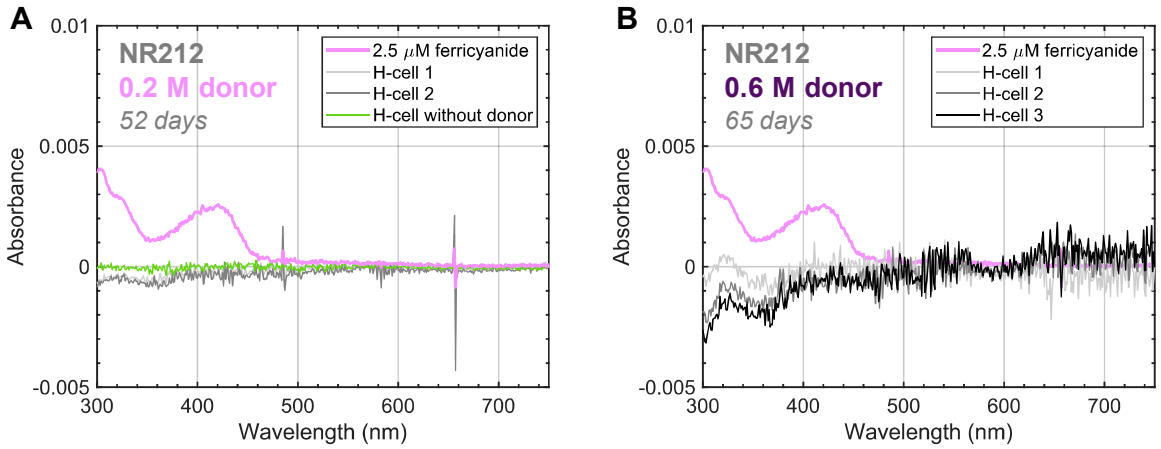

Figure S7: UV-vis absorbance spectra of undiluted H-cell receiving electrolytes after long duration experiments (as specified) for H-cells comprising as-received potassium-exchanged NR212 and potassium-based electrolytes. (a) includes a control experiment where the receiving solution corresponding to the 0.2 M potassium ferricyanide donor was used in both H-cell chambers, with no donor included in either chamber. These results indicate undetectable crossover of potassium ferricyanide at both 0.2 M and 0.6 M concentrations, for experiments lasting longer than 50 days.

Supplementary Discussion 2 - Estimating capacity loss from crossover

In this note, we detail an example calculation to estimate capacity loss from crossover. For simplicity, we assume that species cross from a capacity limiting (donor) electrolyte, driven only by the concentration gradient, to a receiving electrolyte where the concentration of the crossed species is always zero (crossed over material does not accumulate). No other mechanisms of species loss from the donating electrolyte are considered, and the state of charge does not change.

To specify the discharge duration, the ratio of energy to power, we first determine the power achievable at 80 % round-trip energy efficiency. Equation S1 gives round-trip energy efficiency ($RTEE$) as the square of the quotient of discharge cell voltage ($V_{discharge}$) divided by open circuit voltage (OCV) (assuming the voltage efficiency losses are the same upon charge and discharge and the coulombic efficiency is unity). We further assume that all voltage efficiency losses are ohmic in nature, so $V_{discharge}$ is given by OCV minus the product of area-specific resistance (ASR) and current density (j), shown in Equation S2. Applying an ASR of 2 Ω cm^2, corresponding to 2.5 mS cm^{-1} conductivity for a 50 μm thick membrane (if all resistance came from the membrane), and an OCV of 1 V, we solve Equations S1 and S2 for a $V_{discharge}$ of 0.9 V at 0.05 A cm^{-2} current density and 80 % $RTEE$. The product of $V_{discharge}$ and j gives areal power density (p) of 0.045 W cm^{-2}.

$$RTEE = \left(\frac{V_{discharge}}{OCV}\right)^2 \tag{S1}$$

$$V_{discharge} = OCV - j \cdot ASR \tag{S2}$$

We next determine the volumetric energy density (e) of the capacity limiting electrolyte, using equation S3, where n is the number of electrons transferred per molecule ($n = 1$ for

ferri-/ferrocyanide), F is Faraday's constant, and C is molar concentration of active species (here we choose 0.5 M). Upon converting units, we have $e = 0.0134$ Wh cm^{-3}.

$$e = n \cdot F \cdot C \cdot OCV \tag{S3}$$

Energy divided by power of a flow battery system gives discharge duration in units of time. Volumetric energy density divided by areal power density gives discharge duration multiplied by the ratio of membrane area to the volume of the capacity limiting electrolyte, a ratio we call S, shown in Equation S4.

$$discharge\ duration = \frac{e}{p} \cdot S \tag{S4}$$

S is specified for a given e, p, and discharge duration, and here we select a discharge duration of 8 h as a practical specification. Finally, we solve Equation S5, which models crossover by diffusion based on Fick's Law, where t is time, P is the permeability of the membrane to the active species, and l is the membrane thickness.

$$\frac{dC}{dt} = -S \cdot \frac{P}{l} \cdot C \tag{S5}$$

The ratio of concentration of active species at a given time (as crossover has progressed) to the initial concentration is equivalent to the capacity of a flow battery normalized to the initial capacity. Thus, from solving Equation S5, we can estimate 85 % capacity retention after 10 years when diffusion-driven crossover is the only capacity loss, $P = 1 \times 10^{-13}$ cm^2 s^{-1}, $l = 50$ μm, $C = 0.5$ M initially, discharge duration is 8 h, and other parameters are as specified in this note.

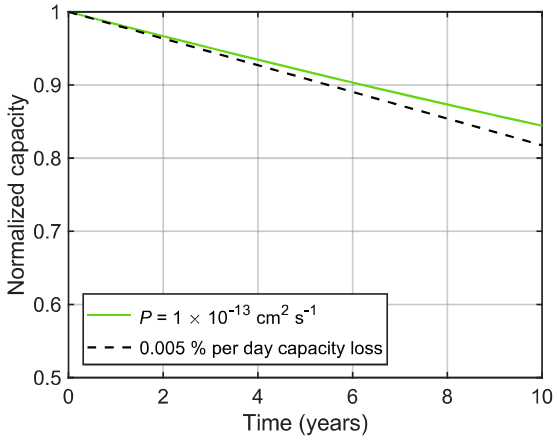

Figure S8: Normalized capacity vs. time in years, determined from the calculation in Supplementary Discussion 2 from solving Equation S5, shows 85 % capacity retention over 10 years when the only mechanism of capacity loss is diffusion-driven crossover with $P = 1 \times 10^{-13}$ cm^2 s^{-1}.

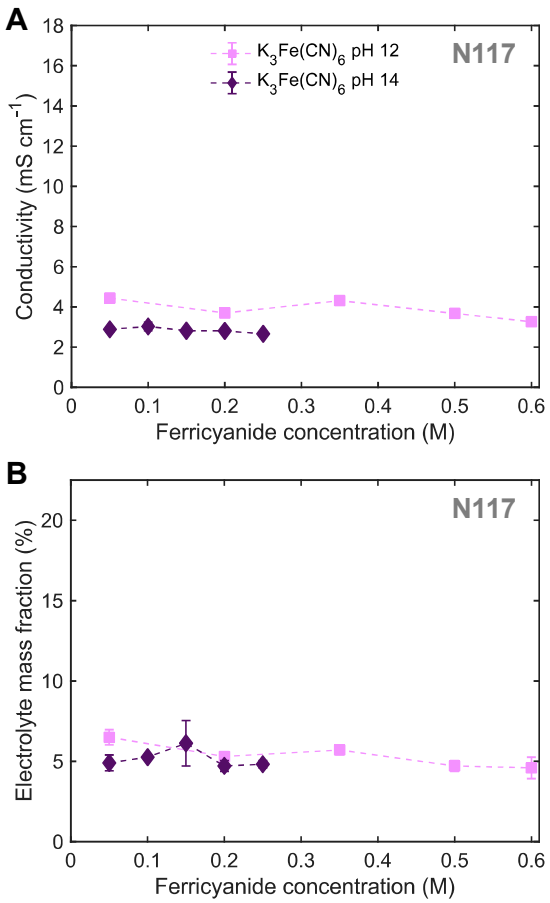

Figure S9: Conductivity (a) and electrolyte mass fraction (b) of as-received Nafion N117 membranes soaked in representative flow battery electrolytes containing potassium ferricyanide (active species) and either 0.01 M (pH 12) or 1 M (pH 14) potassium hydroxide supporting electrolyte.

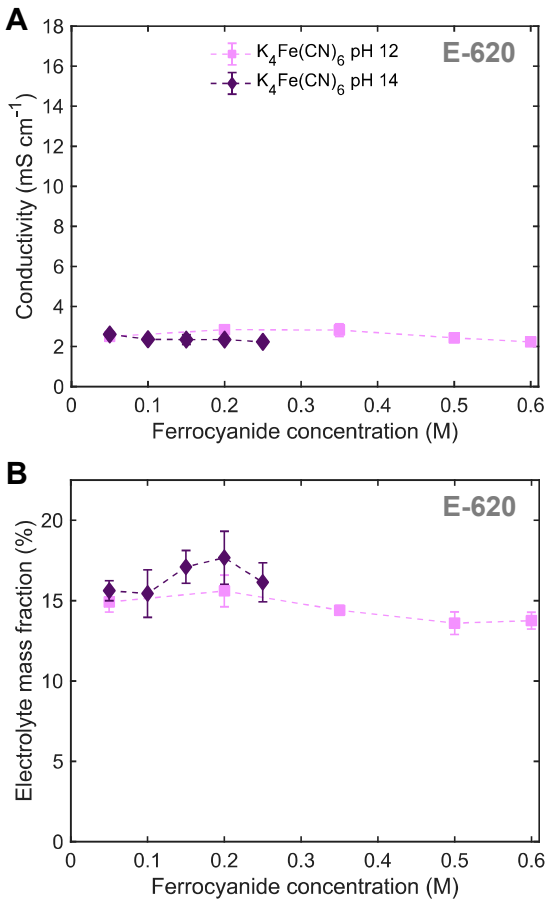

Figure S10: Conductivity (a) and electrolyte mass fraction (b) of as-received E-620 membranes soaked in representative flow battery electrolytes containing potassium ferrocyanide (active species) and either 0.01 M (pH 12) or 1 M (pH 14) potassium hydroxide supporting electrolyte.

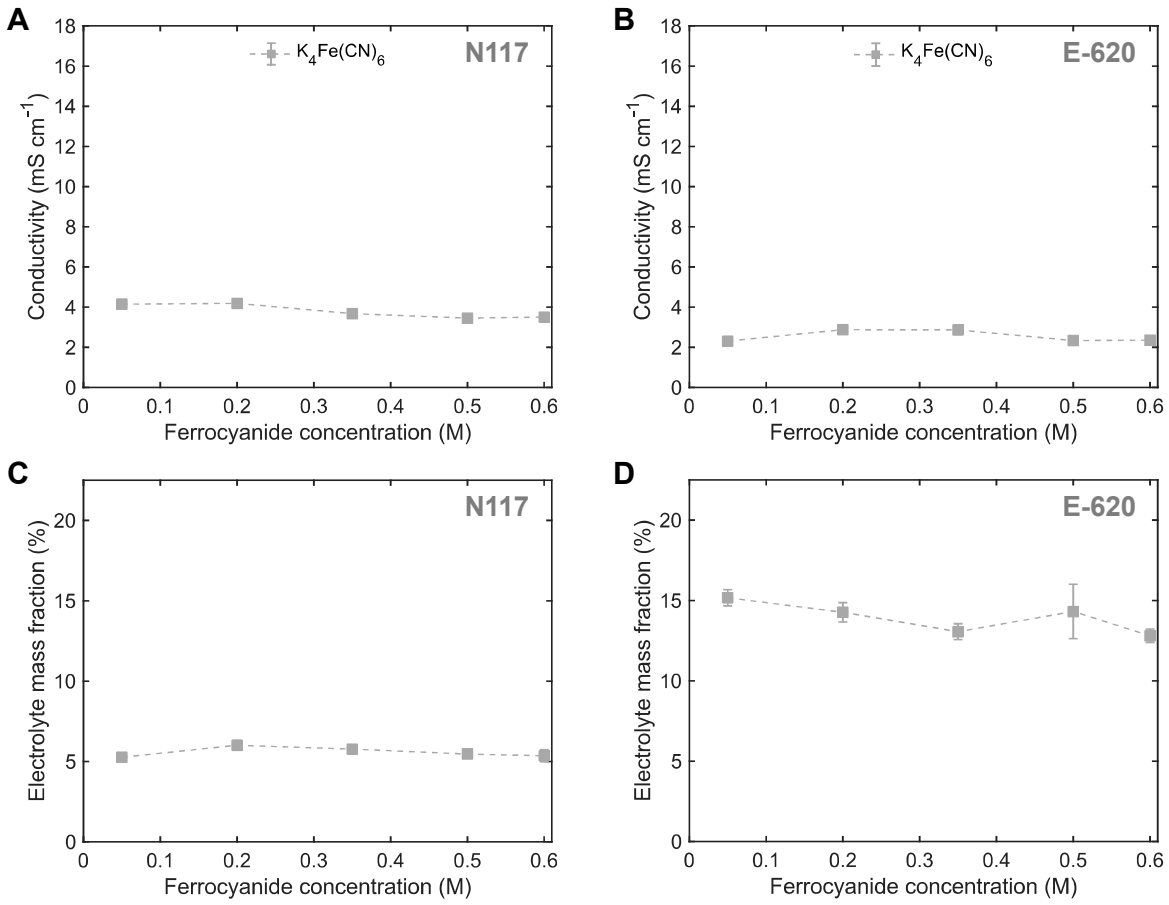

Figure S11: Conductivity (a,b) and electrolyte mass fraction (c,d) of as-received Nafion N117 (a,c) and E-620 (b,d) membranes soaked in representative flow battery electrolytes containing potassium ferrocyanide (active species), without supporting electrolyte. Note that Nafion membranes in this experiment were first potassium exchanged in a separate electrolyte, rinsed in deionized water, and then transferred to the ferrocyanide electrolyte, to avoid the protons in as-received Nafion acidifying the ferrocyanide and generating dangerous HCN.

Table S2: Data from main text Figure 1a,c (MOH concentration abscissa) and main text Figure 5 (concentration of ions abscissa) including conductivity and electrolyte mass fraction of Nafion N117 membranes, pre-treated and as-received, soaked in NaOH or KOH electrolytes.

Membrane, pre-treatment, electrolyte	Symbol	Concentration (M)	Conductivity (mS cm^{-1})	Electrolyte mass fraction (%)	Concentration of ions (M)
Nafion N117, pre-treated, NaOH	△	0.1	10.08 ± 0.06	20.08 ± 0.27	0.2
		1	14.02 ± 0.29	18.44 ± 0.21	2
		2	15.75 ± 0.60	17.85 ± 0.33	4
		3	15.22 ± 1.94	17.20 ± 0.21	6
		4	10.16 ± 0.95	16.52 ± 0.21	8
Nafion N117, as-received, NaOH	▲	0.1	9.75 ± 0.16	15.16 ± 0.05	0.2
		1	10.36 ± 0.07	12.99 ± 0.21	2
		2	10.39 ± 0.88	12.06 ± 0.07	4
		3	9.30 ± 0.91	11.33 ± 0.08	6
		4	8.67 ± 1.14	11.13 ± 0.26	8
Nafion N117, pre-treated, KOH	▽	0.1	8.31 ± 0.27	12.52 ± 0.62	0.2
		1	8.54 ± 0.40	10.72 ± 0.38	2
		2	8.34 ± 0.26	10.13 ± 0.49	4
		3	7.28 ± 0.22	9.51 ± 0.28	6
		4	5.05 ± 0.29	9.57 ± 0.08	8
Nafion N117, as-received, KOH	▼	0.1	5.25 ± 0.03	8.54 ± 0.13	0.2
		1	3.44 ± 0.27	5.82 ± 0.03	2
		2	2.83 ± 0.39	5.18 ± 0.01	4
		3	2.59 ± 0.26	4.72 ± 0.08	6
		4	3.31 ± 0.82	4.38 ± 0.19	8

Table S3: Data from main text Figure 1b,d (MOH concentration abscissa) and main text Figure 6d (concentration of ions abscissa) including conductivity and electrolyte mass fraction of E-620 membranes, as-received, soaked in NaOH or KOH electrolytes.

Membrane, pre-treatment, electrolyte	Symbol	Concentration (M)	Conductivity (mS cm^{-1})	Electrolyte mass fraction (%)	Concentration of ions (M)
E-620, as-received, NaOH	▲	0.1	2.52 ± 0.17	16.00 ± 0.63	0.2
		1	2.74 ± 0.12	16.53 ± 0.59	2
		2	2.43 ± 0.15	16.71 ± 0.72	4
		3	1.96 ± 0.18	16.99 ± 0.64	6
		4	0.94 ± 0.08	18.23 ± 0.95	8
E-620, as-received, KOH	▼	0.1	2.46 ± 0.08	16.73 ± 1.32	0.2
		1	2.89 ± 0.14	18.22 ± 0.16	2
		2	1.48 ± 0.15	18.22 ± 2.33	4
		3	1.43 ± 0.43	17.55 ± 1.30	6
		4	1.37 ± 0.49	20.07 ± 1.17	8

Table S4: Data from main text Figure 3 (ferrocyanide concentration abscissa, pH 12 and pH 14 electrolytes), main text Figure 5 (concentration of ions abscissa), and Figure S11a,c (ferrocyanide concentration abscissa) including conductivity and electrolyte mass fraction of Nafion N117 membranes, as-received, soaked in ferrocyanide-based electrolytes.

Membrane, electrolyte	Symbol	Ferrocyanide concentration (M)	Conductivity (mS cm^{-1})	Electrolyte mass fraction (%)	Concentration of ions (M)
Nafion N117, $Na_4Fe(CN)_6$ pH 12		0.05	8.72 ± 0.22	14.30 ± 0.38	0.27
		0.2	9.69 ± 0.30	13.38 ± 0.16	1.02
		0.35	9.87 ± 0.42	12.85 ± 0.17	1.77
		0.5	9.08 ± 0.11	12.28 ± 0.05	2.52
Nafion N117, $Na_4Fe(CN)_6$ pH 14		0.05	10.36 ± 0.63	12.67 ± 0.21	2.25
		0.1	11.25 ± 1.00	12.67 ± 0.32	2.5
		0.15	10.89 ± 0.75	12.71 ± 0.09	2.75
		0.2	10.89 ± 0.33	12.62 ± 0.25	3
Nafion N117, $K_4Fe(CN)_6$ only		0.05	4.15 ± 0.11	5.26 ± 0.21	0.25
		0.2	4.19 ± 0.12	6.01 ± 0.30	1
		0.35	3.68 ± 0.04	5.77 ± 0.06	1.75
		0.5	3.45 ± 0.11	5.46 ± 0.11	2.5
		0.6	3.50 ± 0.08	5.36 ± 0.37	3
Nafion N117, $K_4Fe(CN)_6$ pH 12		0.05	4.07 ± 0.04	6.40 ± 0.03	0.27
		0.2	3.99 ± 0.18	6.08 ± 0.13	1.02
		0.35	3.91 ± 0.19	6.08 ± 0.14	1.77
		0.5	3.71 ± 0.22	5.48 ± 0.10	2.52
		0.6	3.49 ± 0.26	4.92 ± 0.15	3.02
Nafion N117, $K_4Fe(CN)_6$ pH 14		0.05	3.43 ± 0.06	4.42 ± 0.37	2.25
		0.1	3.30 ± 0.08	4.71 ± 0.19	2.5
		0.15	3.59 ± 0.24	4.53 ± 0.33	2.75
		0.2	3.56 ± 0.65	4.75 ± 0.16	3
		0.25	2.60 ± 0.06	4.56 ± 0.29	3.25

Table S5: Data from Figure S9 (ferricyanide concentration abscissa) including conductivity and electrolyte mass fraction of Nafion N117 membranes, as-received, soaked in ferricyanide-based representative battery electrolytes.

Membrane, electrolyte	Symbol	Ferricyanide concentration (M)	Conductivity (mS cm^{-1})	Electrolyte mass fraction (%)
Nafion N117, $K_3Fe(CN)_6$ pH 12	■	0.05	4.44 ± 0.13	6.50 ± 0.47
		0.2	3.70 ± 0.06	5.30 ± 0.19
		0.35	4.31 ± 0.11	5.71 ± 0.30
		0.5	3.67 ± 0.16	4.71 ± 0.33
		0.6	3.26 ± 0.07	4.59 ± 0.67
Nafion N117, $K_3Fe(CN)_6$ pH 14	◆	0.05	2.89 ± 0.11	4.90 ± 0.49
		0.1	3.03 ± 0.22	5.26 ± 0.12
		0.15	2.81 ± 0.06	6.12 ± 1.42
		0.2	2.81 ± 0.04	4.71 ± 0.34
		0.25	2.66 ± 0.05	4.82 ± 0.23

Table S6: Data from main text Figure 6d (concentration of ions abscissa), Figure S10 (ferrocyanide concentration abscissa, pH 12 and 14 electrolytes), and Figure S11b,d (ferrocyanide concentration abscissa, no supporting electrolyte) including conductivity and electrolyte mass fraction of E-620 membranes, as-received, soaked in ferrocyanide-based representative battery electrolytes.

Membrane, electrolyte	Symbol	Ferrocyanide concentration (M)	Conductivity (mS cm^{-1})	Electrolyte mass fraction (%)	Concentration of ions (M)
E-620, $K_4Fe(CN)_6$ only	■	0.05	2.31 ± 0.02	15.17 ± 0.50	0.25
		0.2	2.87 ± 0.07	14.26 ± 0.60	1
		0.35	2.87 ± 0.16	13.06 ± 0.49	1.75
		0.5	2.34 ± 0.03	14.32 ± 1.69	2.5
		0.6	2.36 ± 0.12	12.80 ± 0.42	3
E-620, $K_4Fe(CN)_6$ pH 12	■	0.05	2.50 ± 0.11	14.92 ± 0.63	0.27
		0.2	2.84 ± 0.14	15.60 ± 0.98	1.02
		0.35	2.82 ± 0.31	14.40 ± 0.31	1.77
		0.5	2.43 ± 0.08	13.60 ± 0.70	2.52
		0.6	2.23 ± 0.16	13.76 ± 0.52	3.02
E-620, $K_4Fe(CN)_6$ pH 14	◆	0.05	2.61 ± 0.13	15.62 ± 0.62	2.25
		0.1	2.36 ± 0.10	15.44 ± 1.48	2.5
		0.15	2.34 ± 0.24	17.10 ± 1.02	2.75
		0.2	2.35 ± 0.09	17.67 ± 1.64	3
		0.25	2.23 ± 0.06	16.14 ± 1.21	3.25

Table S7: Data from main text Figure 6c (fraction of potassium cations abscissa) and Figure S6d (concentration of ions abscissa) including conductivity of E-620 membranes, as-received, soaked in saturated ferrocyanide electrolytes.

Membrane, electrolyte	Symbol	Ferrocyanide concentration (M)	Fraction of potassium cations	Conductivity (mS cm^{-1})	Concentration of ions (M)
E-620, saturated ferrocyanide pH 12	●	0.53	0	3.45 ± 0.10	2.67
		1.34	0.4	0.99 ± 0.36	6.72
		1.5	0.5	0.88 ± 0.07	7.52
		1.33	0.6	0.86 ± 0.28	6.67
		0.7	1	2.92 ± 0.47	3.52
E-620, saturated ferrocyanide pH 14	●	0.2	0	2.65 ± 0.05	3
		0.96	0.4	0.89 ± 0.25	6.8
		1.22	0.5	0.74 ± 0.07	8.1
		0.98	0.6	0.94 ± 0.25	6.9
		0.34	1	2.27 ± 0.60	3.7

References

(1) George, T. Y.; Kerr, E. F.; Haya, N. O.; Alfaraidi, A. M.; Gordon, R. G.; Aziz, M. J. Size and Charge Effects on Crossover of Flow Battery Reactants Evaluated by Quinone Permeabilities Through Nafion. *Journal of the Electrochemical Society* **2023**, *170*, 040509.

(2) Robb, B. H.; George, T. Y.; Davis, C. M.; Tang, Z.; Fujimoto, C. H.; Aziz, M. J.; Marshak, M. P. Sulfonated Diels-Alder Poly(phenylene) Membrane for Efficient Ion-Selective Transport in Aqueous Metalorganic and Organic Redox Flow Batteries. *Journal of The Electrochemical Society* **2023**, *170*, 030515.